

# **WING DESIGN OPTIMIZATION REPORT**

**Calvin Tang**

**June 14, 2024**

**MAE 154B**

# TABLE OF CONTENTS

|              |   |
|--------------|---|
| <b>I.</b>    | <b>SCOPE ... 2</b>  |
| <b>II.</b>   | <b>DESIGN REQUIREMENTS &amp; PARAMETERS ...2</b>                |
| <b>III.</b>  | <b>DEFINING CRITICAL LOADING CONDITIONS ...4</b>                |
|              | A. Introduction to Flight Envelope ... 4                        |
|              | B. PHAA & NHAA Critical Loads ... 5                             |
|              | C. PLAA & NLAA Critical Loads ... 11                            |
|              | D. Gust Loads ... 16  |
| <b>IV.</b>   | <b>WING ANALYSIS PSEUDO CODE ... 19</b>                         |
| <b>V.</b>    | <b>STRESSES ... 20</b>  |
|              | A. Load Distributions ... 20                                    |
|              | B. Buckling Applied Stresses - Stringers and Spar Caps ... 21   |
|              | C. Buckling Applied Stresses - Webs ... 23                      |
| <b>VI.</b>   | <b>CRITICAL STRESSES ... 25</b>                                 |
|              | A. Buckling Failure Stress - Stringers and Spar Caps ... 25     |
|              | B. Buckling Failure Stress - Webs ... 26                        |
|              | C. Curved Panel - Panels ... 27                                 |
| <b>VII.</b>  | <b>FAILURE CRITERIA ... 28</b>                                  |
|              | A. Buckling Failure Criteria - Stringers and Spar Caps ... 28   |
|              | B. Buckling Failure Criteria - Webs ... 28                      |
|              | C. Yield Failure Criteria ... 29                                |
|              | D. Wing Divergence ... 30                                       |
| <b>VIII.</b> | <b>WING OPTIMIZATION ... 30</b>                                 |
| <b>IX.</b>   | <b>FINAL WING DESIGN ... 38</b>                                 |
|              | A. Stringer and Spar Cap Compressive Stresses Mesh Plots ... 41 |
|              | B. Web Shear + Compression Stresses Mesh Plots ... 43           |
|              | C. Nose and Spar Shear + Bending Stresses Mesh Plots ... 46     |
|              | D. Panel Yielding Stresses Mesh Plots ... 47                    |
| <b>X.</b>    | <b>CONCLUSION ... 51</b>  |

## I. SCOPE

This report covers the design of a single-engine utility aircraft wing capable of lifting ~3,200 lbs during flight and the analysis involved to minimize the overall weight of the aircraft's wing structure. NACA 2412 airfoil specifications are referenced for this wing design. Curation of dimensional parameters takes a Monte Carlo approach to converge on an optimal wing design capable of meeting aircraft requirements. A detailed analysis of the wing stresses is performed to ensure critical stresses aren't exceeded and hence validating wing design. This effort is made in accommodation for the requirements defined by Federal Aviation Regulations (FAR) Part 23.

## II. DESIGN REQUIREMENTS & PARAMETERS

*Requirements:*

1. NACA 2412 Airfoil
2. Wing supports maximum total weight of 3,200 lbs
3. Wing support minimum total weight of 1,900 lbs
4. FAR part 23 requirements:
  - a. Limit load factor for utility aircraft: +4.4, -1.76
  - b. 50% factor of safety (ultimate load factor)
  - c. 50 fps gust requirement for cruise speed ( $V_C$ )
  - d. 25 fps gust requirement for dive speed ( $V_D$ )
5. Additional safety margin of 50%

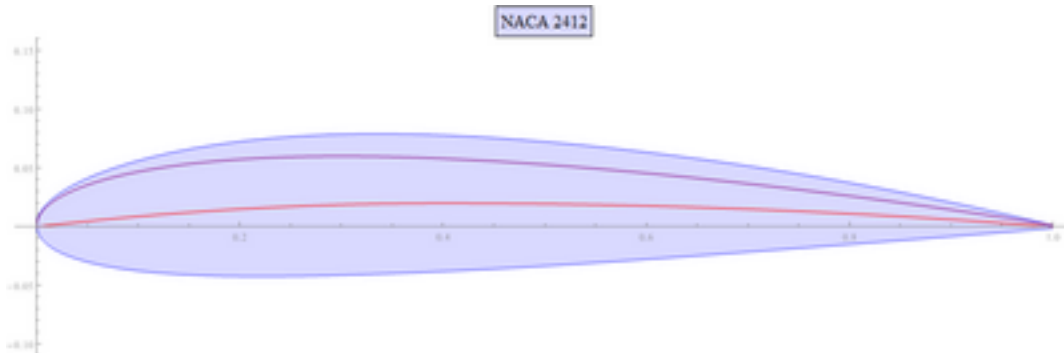


**Figure 1. NACA 2412 Airfoil - Wing Cross Section**

*Fixed Framework:*

1. Chord = 5 ft
2. Semispan = 17 ft
3.  $V_C$  = 230 mph
4.  $V_D$  = 270 mph

*Variable Parameters:*

1. Front/rear spar thickness & location
2. Cross-sectional area & dimensions of spar caps
3. Area & number of stringers
4. Span-wise location & thickness of ribs
5. Skin thickness

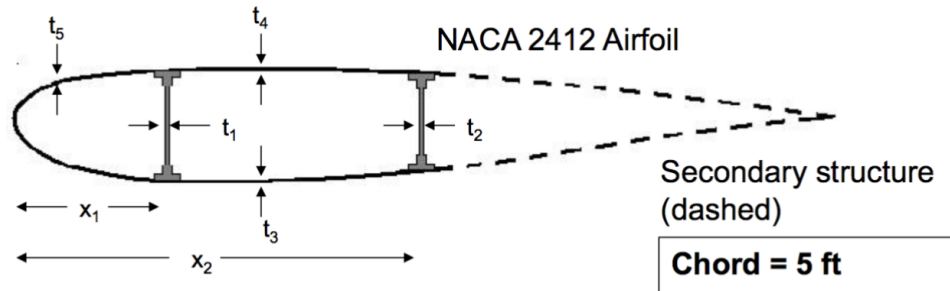


**Figure 2. NACA 2412 Airfoil - Showcase of Variable Parameters**

Base Assumptions:

1. Dynamic viscosity and air density data is referenced at sea level
2. Parasite Drag applied to the wings only
3. 10 LBS per rib
4. Uniform load distribution along span of wing
5. Webs not included in centroid analysis

Other assumptions specified in respective sections

### III. DEFINING CRITICAL LOADING CONDITIONS

#### A. Introduction to Flight Envelope

The design of this wing structure takes a Monte Carlo approach. Simply put, an optimal wing design is achieved through an iterative process of sampling random design parameters, analyzing the diverse outcomes, and refining/repeating the process to converge on ideal results. Before iterating, the operational limitations of the aircraft must be defined to understand the limitations of the wing design.

The operational limitations of the aircraft can be visualized by developing a flight envelope around the wing. This envelope, otherwise interpreted as a V-n diagram, will represent the boundaries within which the aircraft can safely operate defined by velocity ( $V$ ) and load factor ( $n$ ); load factor is defined as the lift to weight ratio. From the V-n diagram, the critical loading conditions within the operational boundaries can be determined. These critical loading conditions are distinguished as Positive High Angle of Attack (PHAA), Negative High Angle of Attack (NHAA), Positive Low Angle of Attack (PLAA), and Negative Low Angle of Attack (NLAA). These critical loading conditions are indicated in Figure 3 at points A, B, C, and D, respectively. Each critical load case is referenced to iteratively pass/fail several randomly generated wing designs.

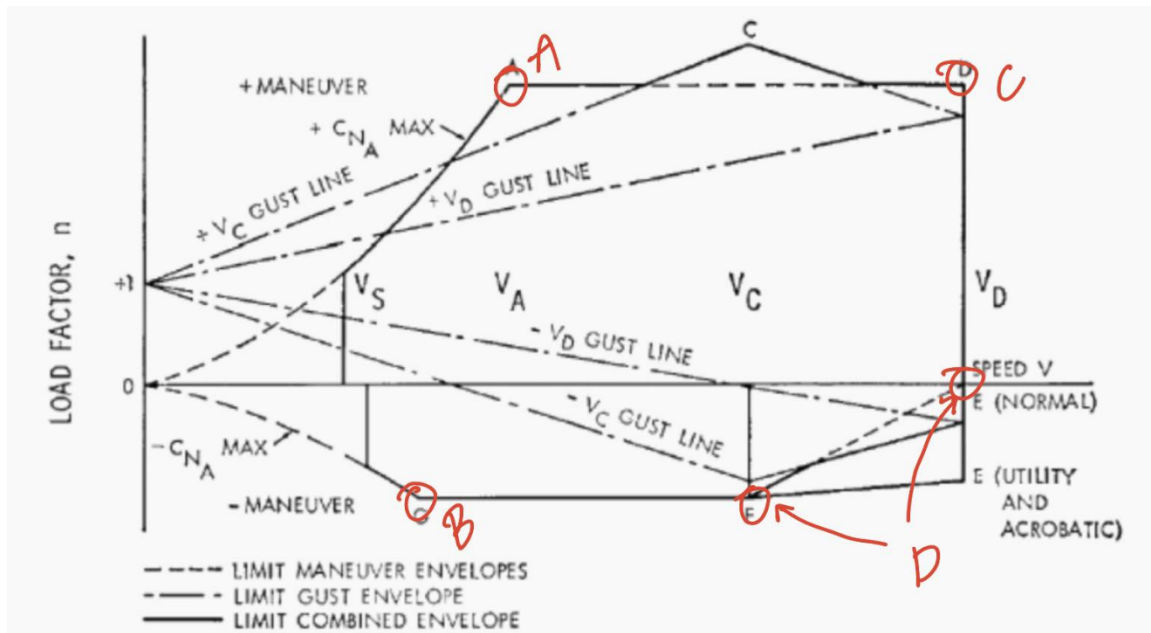


Figure 3. Flight Envelope with noted critical load conditions

## B. PHAA & NHAA Critical Loads

The first step taken to create the V-n diagram is to determine the PHAA load conditions. To start defining this condition, the maximum 2D lift coefficient ( $C_{l,max}$ ) must be found to obtain the maximum 3D lift coefficient ( $C_{L,max}$ ) and maximum 3D drag coefficient ( $C_{D,max}$ ). The NACA 2412 airfoil was simulated using XFOIL, an interactive software for the design and analysis of subsonic isolated airfoils. Figure 5.

showcases the calculations of the Reynolds number implemented in XFOIL with the assumption that dynamic viscosity and air density can be referenced at sea level. As shown in the XFOIL data output in Figure 5,  $C_l$  values were generated corresponding to different Angle of Attack values ( $\alpha$ );  $C_l$  and  $\alpha$  are linearly related. From the XFOIL results, we find that  $C_{l,max} = 1.9714$  at  $\alpha_{l,max} = 20^\circ$ . The following equation is used to solve for  $C_{L,max}$ :

$$C_{L,max} = \frac{C_{l,max}}{1 + \frac{C_{l,max}}{A\pi e}}$$

Given:

- $C_{l,max} = 1.9714$ , 2D maximum lifting coefficient
- $b = 34$  ft, wing span
- $S = 170$  ft<sup>2</sup>, wing area
- $A = \frac{b^2}{S} = 6.8$ , wing aspect ratio
- $e = 0.7$ , Oswald's efficiency factor

Derived from  $C_{l,max}$ , the 3D maximum lifting coefficient  $C_{L,max} = 1.7417$ . This is justified since the 3D lifting coefficient is less than the 2D lifting coefficient since there are more obstructions in a 3D analysis compared to 2D. As previously noted, the limitations of the aircraft limit loading factor (n) is [+4.4, -1.76]. This +4.4 case, reflected in PHAA loading conditions, represents the most extreme loads applied on the wings. To ensure wing stability/performance, we can apply an additional 25% margin to  $C_{L,max}$  and  $\alpha_{l,max}$  to account for this:  $C_{L,max} = 2.1772$ ,  $\alpha_{l,max} = 25^\circ$ .

$$\rho @ \text{sea level} = 23.77 \times 10^{-4} \frac{\text{slug}}{\text{ft}^3}; \mu @ \text{sea level} = 3.737 \times 10^{-7} \frac{\text{slug}}{\text{ft} \cdot \text{s}}$$

$$V = V_{cruise} = 230 \text{ mph} = 337.333 \text{ ft/s}; L = \text{chord length} = 5 \text{ ft}$$

$$Re = \frac{\rho V L}{\mu} = \frac{(23.77 \times 10^{-4} \frac{\text{slug}}{\text{ft}^3})(337.333 \frac{\text{ft/s}}{\text{s}})(5 \text{ ft})}{3.737 \times 10^{-7} \frac{\text{slug}}{\text{ft} \cdot \text{s}}} \approx 10,728,399$$

Figure 4. Calculations of Reynolds Numbers

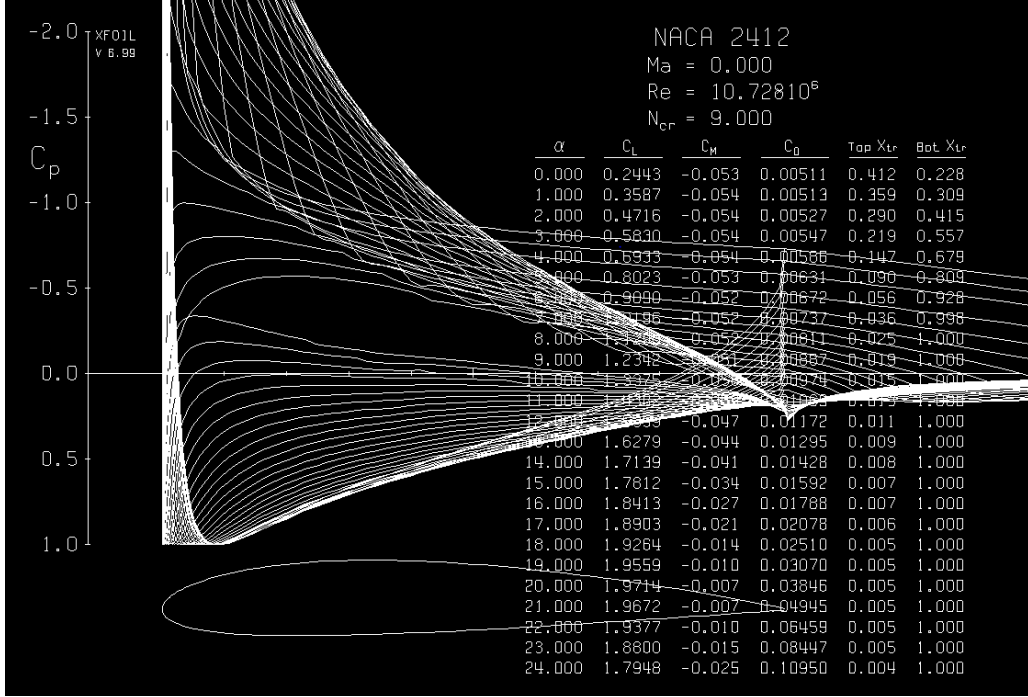


**Figure 5. NACA 2412 XFOIL Data, Emphasis on  $C_{L,\max}$  vs.  $\alpha$**

With  $C_{L,\max}$  known, the maximum 3D drag coefficient ( $C_{D,\max}$ ) for the wing can be found. The 3D drag coefficient ( $C_D$ ) is defined by the sum of Parasite Drag ( $C_{DP}$ ) and Induced Drag ( $C_{Di}$ ). Parasite Drag is an aerodynamic drag produced when an object moves through fluid. In this case the Parasite Drag is primarily affected by the NACA 2412 airfoil shape. Induced Drag is the drag inevitably influenced by the generation of lift. The pressure difference that generates lift leads to the generation of vortices about the wing tip (flow from the bottom to the top of the wing) that causes upwash outside and downwash inside the wing's span. The downwash effect rotates the lift vector in the direction of free-streaming air (Induced Drag). The following shows the equations and given knowns used to solve for the NACA 2412  $C_{D,\max}$ :

$$C_D = C_{DP} + C_{Di}$$

$$C_{DP} = \sum_{i=1}^{\text{comp\#}} \frac{K_i Q_i C_{f,i} S_{wet,i}}{S_{ref}} + C_{D,misc} + C_{D,L\&P}$$

$$C_{Di} = \frac{(C_{L,\max})^2}{\pi A e}$$

Given:

- $C_f = \frac{0.455}{(\log_{10} Re)^{2.58} (1+0.144M^2)^{0.65}}$ , Skin friction eq.
- $K = [1 + \frac{0.6}{(x/c)_m} (\frac{t}{c}) + 100(\frac{t}{c})^4] [1.34M^{0.18} \cos(\Lambda_m)^{0.28}]$ , Form factor eq.
- $Re = 10,728,399$ , Reynold's number
- $M = 0.2998$ , Mach #

- $(\frac{t}{c}) = 0.12$ , Airfoil thickness at max camber represented as % chord
- $(\frac{x}{c})_m = 0.30$ , Position of max camber represented as % chord
- $\Lambda_m = 0^\circ$ , Wing sweep angle
- $Q_i = 1$ , Interference factor
- $S_{ref} = 170 \text{ ft}^2$ , Reference area (wing area)
- $C_{D,misc}$ , Additional miscellaneous drag terms
- $C_{D,L\&P}$ , Leakage and protuberance
- $A = \frac{b^2}{S} = 6.8$ , Wing aspect ratio
- $e = 0.7$ , Oswald's efficiency factor

It is assumed that Mach # is derived from cruise speed ( $V_c$ ) and that there is no interference between aircraft components ( $Q_i = 1$ ). For this calculation, it is also assumed that  $C_{D,misc}$  and  $C_{D,L\&P}$  can be neglected since their values are minuscule. It can be concluded that  $C_{DP} = 0.0043$  and  $C_i = 0.3169$ . These calculations indicate that the Induced Drag is greater than the Parasite Drag; this is justified since the aircraft has a larger wing span which causes more downwash. Summing these terms, we find that  $C_{D,max} = 0.3213$ .

With  $C_{L,max}$  and  $C_{D,max}$  fully defined at  $\alpha = 25^\circ$ , the maximum coefficient of the Normal load ( $C_{N,max}$ ) and the maximum coefficient of the X load ( $C_{X,max}$ ) can be derived using the following equations:

$$\begin{aligned} C_{N,max} &= C_{L,max} \cos(\alpha) + C_{D,max} \sin(\alpha) \\ C_{X,max} &= C_{D,max} \cos(\alpha) - C_{N,max} \sin(\alpha) \end{aligned}$$

$C_{N,max} = 2.1090$  and  $C_{X,max} = 0.6289$ . These loading coefficients are significant for defining the constrained load factor boundary of the flight envelope building up to PHAA. When flying at low speeds, high load factors require high lift coefficients. Hence, the load factor is constrained by maximum lift coefficient. The load factor equation used to define this curved boundary in Figure 6 is used to determine the velocity (V) required to reach limit load factor +4.4:

$$n = \frac{\frac{1}{2} \rho V^2 S C_{N,max}}{W}$$

Given:

- $\rho = 23.77 \times 10^{-4} \frac{\text{slug}}{\text{ft}^2}$ , air density at sea level
- $n = +4.4$ , PHAA load factor
- $S = 170 \text{ ft}^2$ , Wing area
- $W = 3200 \text{ lbf}$ , Max weight of aircraft

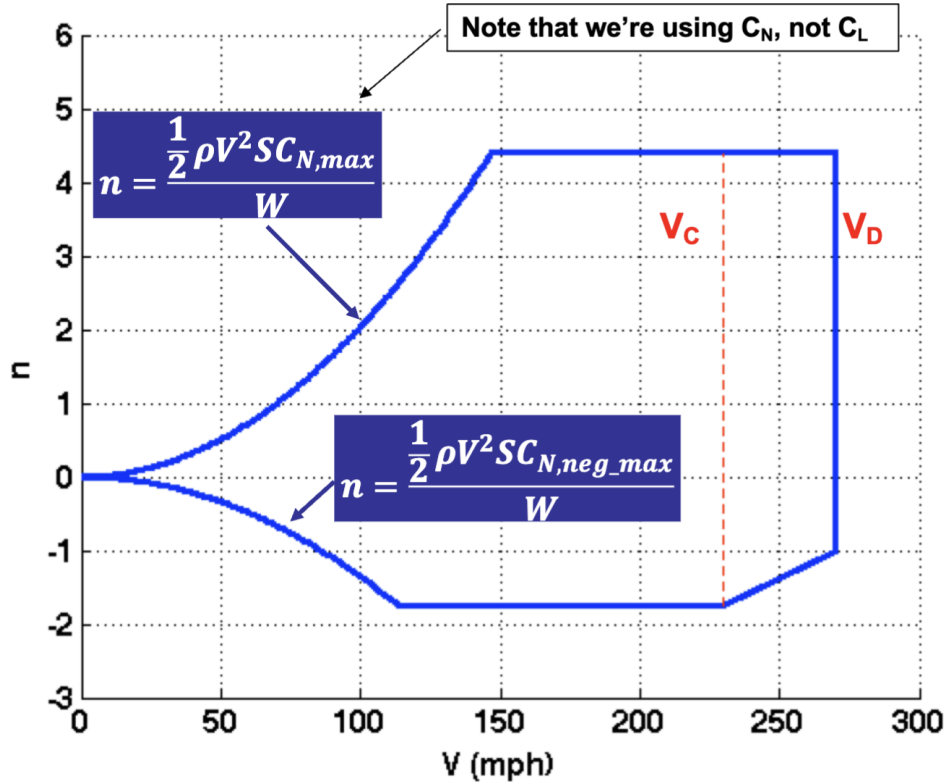


**Figure 6. Sample V-n Diagram - Highlighting Limit Loading Equation to Define Envelope Boundary**

$V = 181.7769 \text{ ft/s} = 123.9388 \text{ mph}$ . The load coefficients and the minimum velocity required to reach critical limit load factor +4.4 determines the critical loads applied directly normal and parallel to the wing's surface for PHAA:  $F_N$  and  $F_X$  referenced in Figure 7. The Lift and Drag forces applied at the  $\alpha = 25^\circ$  can be calculated and compared to  $F_N$  and  $F_X$  to verify load magnitudes:

$$F_N = \frac{1}{2} \rho V^2 S C_{N,max} = 4.4 * W$$

$$F_X = \frac{1}{2} \rho V^2 S C_{X,max}$$

$$L = \frac{1}{2} \rho V^2 S C_L$$

$$D = \frac{1}{2} \rho V^2 S C_D$$

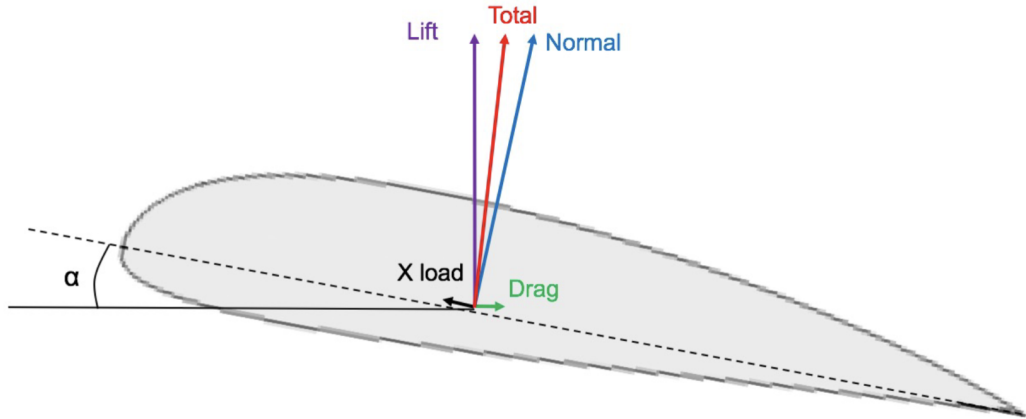


**Figure 7. Illustration of  $F_N$  and  $F_X$  vs. Lift and Drag**

$F_N = 14080 \text{ lbf}$  and  $F_X = -4199.1542 \text{ lbf}$ .  $L = 14535.4529 \text{ lbf}$  and  $D = 2144.7389 \text{ lbf}$ . The magnitudes for these sets of forces on the wing are proportional relative to the angle of attack. Note:  $F_N$  and  $F_X$  values are referenced later to solve and identify stresses along the span of the wing for the PHAA load condition.

This process will be repeated to characterize the critical load condition for NHAA. As aforementioned, PHAA represents the most extreme critical load condition since it encapsulates a combination of the highest limit load factor +4.4 and the highest drag force due to the high angle of attack. Hence the NHAA critical load conditions can be defined without applying an additional 25% margin that was included for PHAA. Associated parameters for PHAA and NHAA critical load conditions are summarized in Table 1.

|                           | PHAA        | NHAA        |
|---------------------------|-------------|-------------|
| n                         | +4.4        | -1.76       |
| C <sub>L,max</sub>        | 1.9714      | 1.9714      |
| α                         | 25°         | 20°         |
| C <sub>L,max</sub>        | 1.7417      | 1.7417      |
| α (+25%)                  | 25°         | —           |
| C <sub>L,max</sub> (+25%) | 2.1772      | —           |
| C <sub>D,max</sub>        | 0.3213      | 0.2071      |
| C <sub>N,max</sub>        | 2.1090      | 1.7076      |
| C <sub>X,max</sub>        | -0.6289     | -0.4011     |
| V [mph]                   | 123.9388    | 87.1132     |
| F <sub>Z</sub> [lbf]      | 14,080      | 5,632       |
| F <sub>X</sub> [lbf]      | -4,199.1542 | -1,322.8497 |
| C <sub>M</sub>            | -0.007      | -0.007      |
| M <sub>y</sub> [lbf ft]   | -233.6649   | -115.4381   |

**Table 1. Define PHAA & NHAA critical load conditions**

In Table 1, the pitching moment coefficient (C<sub>M</sub>) denoted and used to determine the pitching moment (M<sub>y</sub>) of the airfoil cross-section. The pitching moment is later used to evaluate the stresses applied to wing panels. M<sub>y</sub> derived using the following equation using corresponding values from Table 1:

$$M_y = \frac{1}{2} \rho V^2 S \bar{c} C_M$$

### C. PLAA & NLAA Critical Loads

For PHAA and NHAA, the critical loads ( $F_N$  &  $F_X$ ) were determined using the angle of attack with the highest lift coefficient. However, the same process cannot be repeated for load conditions PLAA and NLAA since the angle of attack is undefined. To solve for the PLAA and NLAA critical loads ( $F_N$  &  $F_X$ ) on the wing, we must work backwards by first defining  $C_N$ . Beginning with PLAA, the critical load condition is defined by the lowest angle of attack within dive speed that achieves +4.4 limit load factor in the flight envelope.  $C_N$  can be solved using the constrained load factor equation:

$$n = \frac{\frac{1}{2} \rho V^2 S C_N}{W}$$

Given:

- $\rho = 23.77 \times 10^{-4} \frac{\text{slug ft}}{\text{s}^2}$ , air density at sea level
- $n = +4.4$ , PLAA load factor
- $S = 170 \text{ ft}^2$ , Wing reference area
- $W = 3200 \text{ lbf}$ , Max weight of aircraft
- $V = 270 \text{ mph}$ , Dive speed corresponding to PLAA condition

$C_N = 0.4444$ . As previously mentioned, we solve for PHAA and NHAA critical loads starting with XFOIL-acquired  $\alpha$  and  $C_l$  to generate  $C_L$ ,  $C_D$ ,  $C_N$ ,  $C_X$ ,  $F_N$ , and  $F_X$  values. Working backwards for PLAA, the  $C_l$ ,  $C_L$ ,  $C_D$ , and  $C_X$  values corresponding to the calculated  $C_N$  are derived by iteratively simulating several  $\alpha$  cases. Table 2 exhibits the iterated XFOIL simulation data used to converge on  $C_N = 0.4444$  for PLAA, and all coefficients corresponding to  $C_N$ . All corresponding coefficients are determined using previously used methods/equations.  $C_N$  and  $C_X$  is later used for calculating  $F_N$  and  $F_X$  critical loads for PLAA.

| <b>a</b> | <b>C,I</b> | <b>C,L</b> | <b>C,DP</b> | <b>C,Di</b> | <b>C,D</b> | <b>C,N</b> | <b>C,X</b> | <b>C,M</b> |
|----------|------------|------------|-------------|-------------|------------|------------|------------|------------|
| 0        | 0.3084     | 0.3022     | 0.0043      | 0.0061      | 0.0104     | 0.3022     | 0.0104     |            |
| 1        | 0.3818     | 0.3723     | 0.0043      | 0.0093      | 0.0135     | 0.3725     | 0.0070     |            |
| 1.8      | 0.4492     | 0.4361     | 0.0043      | 0.0127      | 0.0170     | 0.4364     | 0.0033     |            |
| 1.87     | 0.4572     | 0.4436     | 0.0043      | 0.0132      | 0.0174     | 0.4440     | 0.0029     |            |
| 1.871    | 0.4573     | 0.4437     | 0.0043      | 0.0132      | 0.0174     | 0.4441     | 0.0029     |            |
| 1.872    | 0.4574     | 0.4438     | 0.0043      | 0.0132      | 0.0174     | 0.4442     | 0.0029     |            |
| 1.873    | 0.4576     | 0.4440     | 0.0043      | 0.0132      | 0.0174     | 0.4444     | 0.0029     | -0.054     |
| 1.874    | 0.4577     | 0.4441     | 0.0043      | 0.0132      | 0.0175     | 0.4444     | 0.0029     |            |
| 1.875    | 0.4577     | 0.4441     | 0.0043      | 0.0132      | 0.0175     | 0.4444     | 0.0029     |            |
| 1.876    | 0.4579     | 0.4443     | 0.0043      | 0.0132      | 0.0175     | 0.4446     | 0.0029     |            |
| 1.877    | 0.4579     | 0.4443     | 0.0043      | 0.0132      | 0.0175     | 0.4446     | 0.0029     |            |
| 1.878    | 0.4581     | 0.4445     | 0.0043      | 0.0132      | 0.0175     | 0.4448     | 0.0029     |            |
| 1.879    | 0.4581     | 0.4445     | 0.0043      | 0.0132      | 0.0175     | 0.4448     | 0.0029     |            |
| 1.88     | 0.4583     | 0.4447     | 0.0043      | 0.0132      | 0.0175     | 0.4450     | 0.0029     |            |
| 1.9      | 0.4606     | 0.4468     | 0.0043      | 0.0134      | 0.0176     | 0.4472     | 0.0028     |            |
| 2        | 0.4716     | 0.4572     | 0.0043      | 0.0140      | 0.0182     | 0.4575     | 0.0023     |            |
| 3        | 0.583      | 0.5611     | 0.0043      | 0.0211      | 0.0253     | 0.5617     | -0.0041    |            |
| 4        | 0.6933     | 0.6626     | 0.0043      | 0.0294      | 0.0336     | 0.6633     | -0.0127    |            |
| 5        | 0.8023     | 0.7614     | 0.0043      | 0.0388      | 0.0430     | 0.7623     | -0.0235    |            |

**Table 2. PLAA XFOIL Simulation Dataset -  $C_N$  and Corresponding Coefficients**

The same iterative process is used for the NLAA critical loading conditions. However, NHAA is distinguished between two different critical loading conditions:  $n = -1.76$  at  $V_c$  and  $n = -1.00$  at  $V_D$  denoted as NHAA 1 and NHAA 2, respectively. Both  $C_N$  values are solved using the constrained load factor equation in Figure 7. Tables 3 & 4 show the iterated XFOIL simulation data used to converge on  $C_N = -0.2450$  and  $C_N = -0.1009$  for NLAA 1 and NHAA 2, and all coefficients corresponding to their respective  $C_N$ . Corresponding parameters for PLAA, NLAA 1, and NLAA 2 critical load conditions are summarized in Table 5.

| <b>a</b> | <b>C,I</b> | <b>C,L</b> | <b>C,DP</b> | <b>C,Di</b> | <b>C,D</b> | <b>C,N</b> | <b>C,X</b> | <b>C,M</b> |
|----------|------------|------------|-------------|-------------|------------|------------|------------|------------|
| -4.27    | -0.2462    | -0.2503    | 0.0043      | 0.0042      | 0.0085     | -0.2503    | -0.0102    |            |
| -4.26    | -0.2451    | -0.2492    | 0.0043      | 0.0042      | 0.0084     | -0.2491    | -0.0101    |            |
| -4.25    | -0.244     | -0.2480    | 0.0043      | 0.0041      | 0.0084     | -0.2480    | -0.0100    |            |
| -4.24    | -0.2428    | -0.2468    | 0.0043      | 0.0041      | 0.0083     | -0.2467    | -0.0099    |            |
| -4.23    | -0.2417    | -0.2457    | 0.0043      | 0.0040      | 0.0083     | -0.2456    | -0.0098    |            |
| -4.229   | -0.2416    | -0.2456    | 0.0043      | 0.0040      | 0.0083     | -0.2455    | -0.0098    |            |
| -4.228   | -0.2414    | -0.2454    | 0.0043      | 0.0040      | 0.0083     | -0.2453    | -0.0098    |            |
| -4.227   | -0.2413    | -0.2453    | 0.0043      | 0.0040      | 0.0083     | -0.2452    | -0.0098    |            |
| -4.226   | -0.2412    | -0.2452    | 0.0043      | 0.0040      | 0.0083     | -0.2451    | -0.0098    |            |
| -4.225   | -0.2411    | -0.2451    | 0.0043      | 0.0040      | 0.0083     | -0.2450    | -0.0098    | -0.051     |
| -4.224   | -0.241     | -0.2449    | 0.0043      | 0.0040      | 0.0083     | -0.2449    | -0.0098    |            |
| -4.223   | -0.2409    | -0.2448    | 0.0043      | 0.0040      | 0.0083     | -0.2448    | -0.0098    |            |
| -4.222   | -0.2408    | -0.2447    | 0.0043      | 0.0040      | 0.0083     | -0.2447    | -0.0098    |            |
| -4.221   | -0.2406    | -0.2445    | 0.0043      | 0.0040      | 0.0083     | -0.2445    | -0.0098    |            |
| -4.22    | -0.2405    | -0.2444    | 0.0043      | 0.0040      | 0.0083     | -0.2444    | -0.0098    |            |
| -4.21    | -0.2394    | -0.2433    | 0.0043      | 0.0040      | 0.0082     | -0.2432    | -0.0097    |            |
| -4.2     | -0.2382    | -0.2421    | 0.0043      | 0.0039      | 0.0082     | -0.2420    | -0.0096    |            |
| -4.1     | -0.2258    | -0.2293    | 0.0043      | 0.0035      | 0.0078     | -0.2292    | -0.0086    |            |
| -4       | -0.2153    | -0.2184    | 0.0043      | 0.0032      | 0.0075     | -0.2184    | -0.0078    |            |

**Table 3. NLAA 1 XFOIL Simulation Dataset - C<sub>N</sub> and Corresponding Coefficients**

| <b>a</b>      | <b>C,I</b>     | <b>C,L</b>     | <b>C,DP</b>   | <b>C,Di</b>   | <b>C,D</b>    | <b>C,N</b>     | <b>C,X</b>     | <b>C,M</b>    |
|---------------|----------------|----------------|---------------|---------------|---------------|----------------|----------------|---------------|
| -5            | -0.3296        | -0.3370        | 0.0043        | 0.0076        | 0.0119        | -0.3368        | -0.0176        |               |
| -4            | -0.2153        | -0.2184        | 0.0043        | 0.0032        | 0.0075        | -0.2184        | -0.0078        |               |
| -3            | -0.1008        | -0.1015        | 0.0043        | 0.0007        | 0.0050        | -0.1016        | -0.0004        |               |
| -2.999        | -0.1007        | -0.1014        | 0.0043        | 0.0007        | 0.0049        | -0.1015        | -0.0004        |               |
| -2.998        | -0.1006        | -0.1013        | 0.0043        | 0.0007        | 0.0049        | -0.1014        | -0.0004        |               |
| -2.997        | -0.1004        | -0.1011        | 0.0043        | 0.0007        | 0.0049        | -0.1012        | -0.0003        |               |
| -2.996        | -0.1003        | -0.1010        | 0.0043        | 0.0007        | 0.0049        | -0.1011        | -0.0003        |               |
| <b>-2.995</b> | <b>-0.1002</b> | <b>-0.1009</b> | <b>0.0043</b> | <b>0.0007</b> | <b>0.0049</b> | <b>-0.1009</b> | <b>-0.0003</b> | <b>-0.052</b> |
| -2.994        | -0.1001        | -0.1008        | 0.0043        | 0.0007        | 0.0049        | -0.1009        | -0.0003        |               |
| -2.993        | -0.1           | -0.1007        | 0.0043        | 0.0007        | 0.0049        | -0.1008        | -0.0003        |               |
| -2.992        | -0.0999        | -0.1006        | 0.0043        | 0.0007        | 0.0049        | -0.1007        | -0.0003        |               |
| -2.991        | -0.0997        | -0.1004        | 0.0043        | 0.0007        | 0.0049        | -0.1005        | -0.0003        |               |
| -2.99         | -0.0996        | -0.1003        | 0.0043        | 0.0007        | 0.0049        | -0.1004        | -0.0003        |               |
| -2.9          | -0.0892        | -0.0897        | 0.0043        | 0.0005        | 0.0048        | -0.0899        | 0.0003         |               |
| -2            | 0.0141         | 0.0141         | 0.0043        | 0.0000        | 0.0043        | 0.0139         | 0.0048         |               |
| -1            | 0.1291         | 0.1280         | 0.0043        | 0.0011        | 0.0054        | 0.1279         | 0.0076         |               |
| 0             | 0.3084         | 0.3022         | 0.0043        | 0.0061        | 0.0104        | 0.3022         | 0.0104         |               |

**Table 4. NLAA 2 XFOIL Simulation Dataset - C<sub>N</sub> and Corresponding Coefficients**

|                         | PLAA    | NLAA 1    | NLAA 2  |
|-------------------------|---------|-----------|---------|
| n                       | +4.4    | -1.76     | -1      |
| C <sub>L,max</sub>      | 0.4576  | -0.2411   | -0.1002 |
| α                       | 1.873°  | -4.225    | -2.995  |
| C <sub>L,max</sub>      | 0.4440  | -0.2451   | -0.1009 |
| C <sub>D,max</sub>      | 0.0174  | 0.0083    | 0.0049  |
| C <sub>N,max</sub>      | 0.4444  | -0.2449   | -0.1009 |
| C <sub>X,max</sub>      | 0.0029  | -0.0097   | -0.0003 |
| V [mph]                 | 270     | 230       | 270     |
| F <sub>Z</sub> [lbf]    | 14,080  | -5,632    | -3200   |
| F <sub>X</sub> [lbf]    | 92.6309 | -225.2942 | -7.7114 |
| C <sub>M</sub>          | -0.054  | -0.051    | -0.052  |
| M <sub>y</sub> [lbf ft] | -8,554  | -8,079    | -5,978  |

**Table 5. Define PLAA, NLAA 1, NLAA 2 Critical Load Conditions**

Compared to the High Angle of Attack critical loading conditions, the Low Angle of Attack values result in a significantly lower applied drag. This validates the calculated critical load condition data since the increase in angle of attack against free stream velocity will naturally incite an increase in lift & drag.

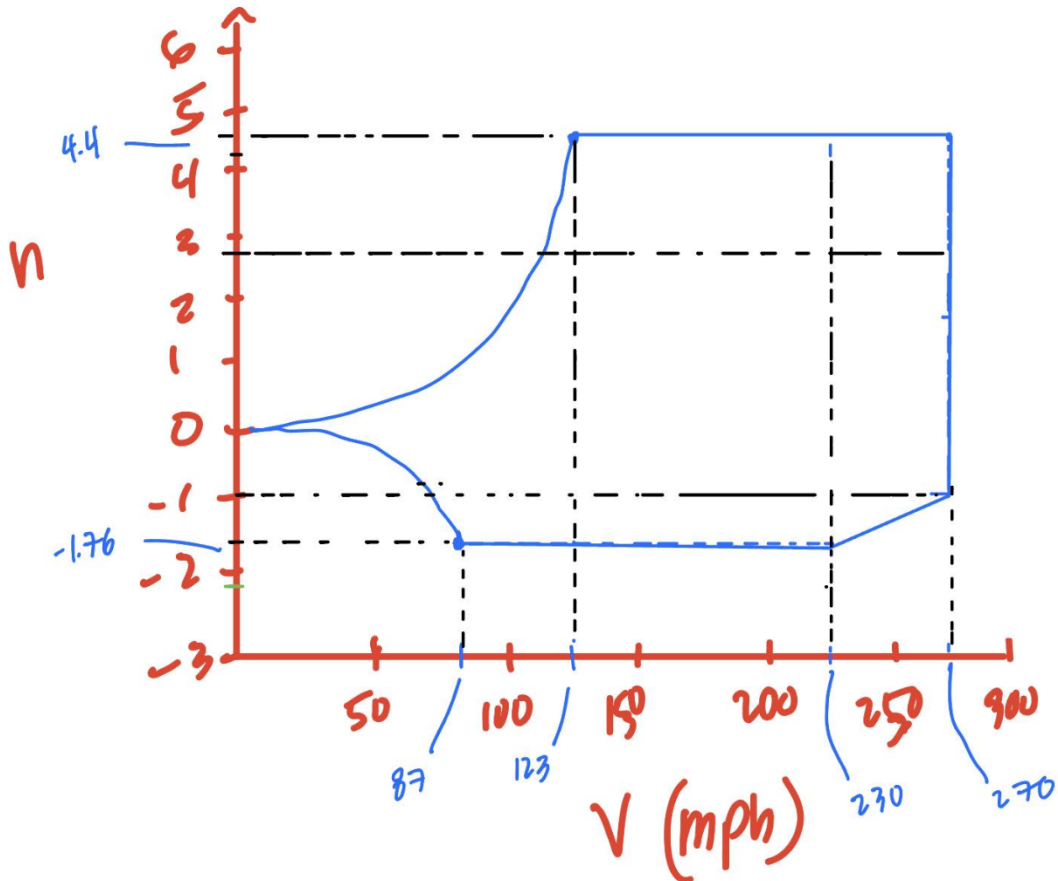


**Figure 8. Flight Envelope without Gust Load**

#### D. Gust Loads

Lastly, to fully define the flight envelope for the wing, the gust loads causing a sudden increase in angle of attack must be accommodated. The change in the angle of attack is based on the ratio of the gust velocity and the aircraft forward velocity. This change in angle of attack ( $\Delta\alpha$ ) directly impacts the change in lift ( $\Delta L$ ) and thus the change in limit load ( $\Delta n$ ) on our V-n diagram at cruise speed and dive speed. Gust load effects are illustrated below:

$$\begin{aligned}\Delta\alpha &= \frac{V_{gust}}{V} \\ \Delta L &= \frac{1}{2} \rho V^2 S C_{L,\alpha} \Delta\alpha \\ \Delta n &= \frac{\rho S C_{L,\alpha} V_{gust} V k}{2W}\end{aligned}$$

Where,

- $V_{gust,c} = 50$  fps, FAR 23 Gust condition at cruise speed
- $V_{gust,d} = 25$  fps, FAR 23 Gust condition at dive speed
- $V$ , velocity at cruise or dive speed
- $C_{L,\alpha} = 4.1242$ , lift coefficient & angle of attack slope (derived from XFOIL)

- $S = 170 \text{ ft}^2$ , Wing reference area
- $\rho = 23.77 \times 10^{-4} \frac{\text{slug ft}}{\text{s}^2}$ , air density at sea level
- $W = 3200 \text{ lbf}$ , Max weight of aircraft
- $k$  = gust alleviation factor

For this gust load analysis, sharp-edge gust loads are not assumed. In reality, gust loads applied onto the wing are rather gradual rather than immediate as depicted in Figure 9. To accommodate for this, the gust alleviation factor ( $k$ ) is included in the change in limit load factor equation above. The gust alleviation factor is solved using the equations below:

$$k = \frac{0.88\mu}{5.3+\mu}$$

$$\mu = \frac{2(W/S)}{\rho g \bar{c} C_{L,\alpha}}$$

Given,

- $g = 32.1740 \frac{\text{ft}}{\text{s}^2}$ , gravity
- $\bar{c} = 5 \text{ ft}$ , chord length

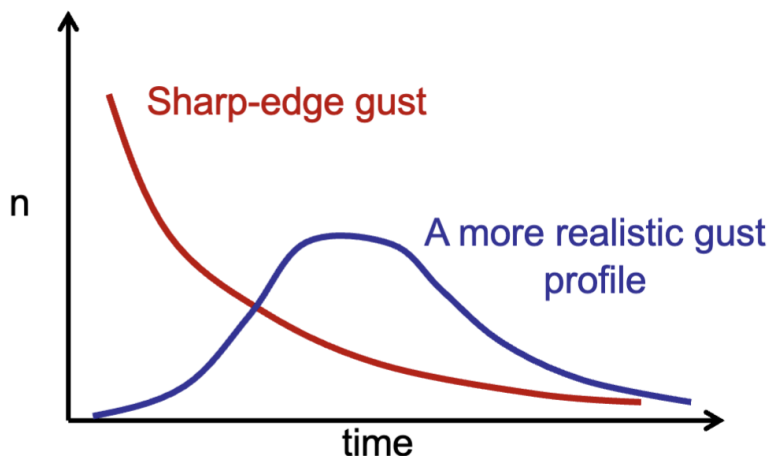


**Figure 9. Illustration of realistic vs. sharp-edge gust loads**

Since the aircraft in context is regularly operating at  $n = 1$ ,  $\Delta n$  must be considered for gust loads bidirectionally ( $\pm \Delta n$ ) as portrayed on the V-n diagram in Figure 10.

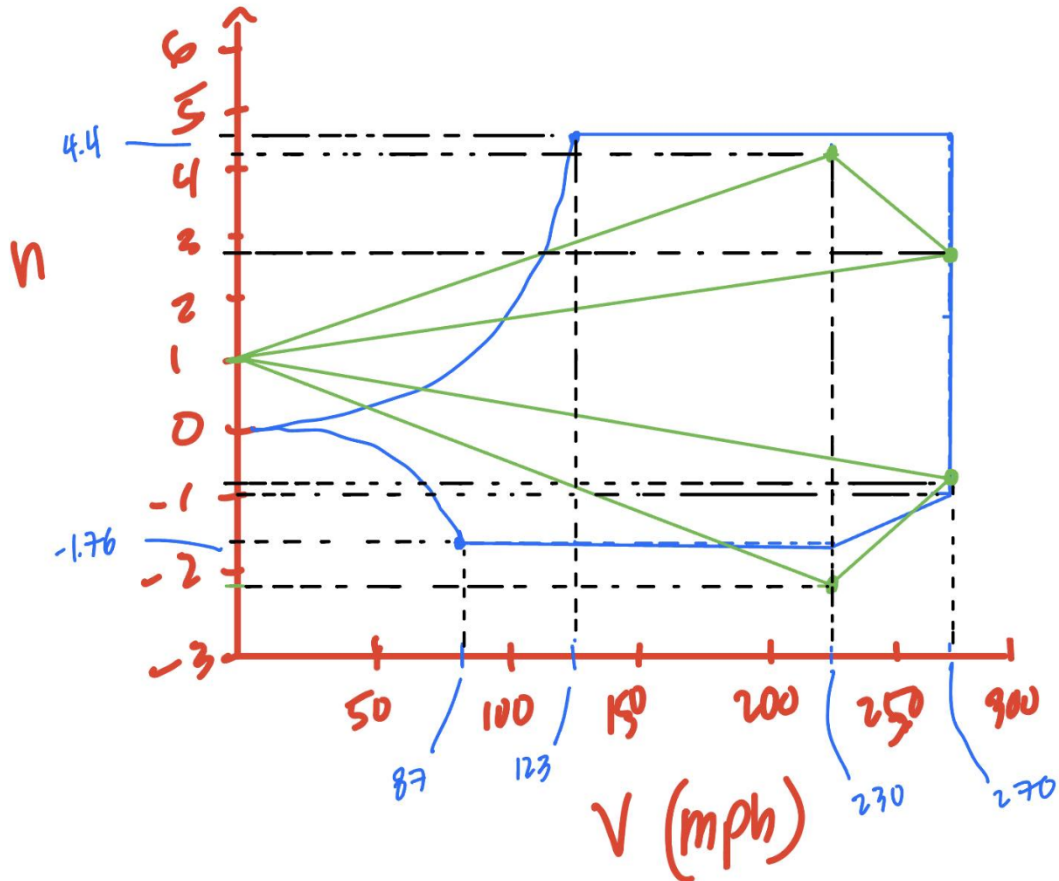


**Figure 10. V-n diagram with gust loads**

From this fully-defined V-n diagram, it is observed that the  $+\Delta n$  critical loads for  $V_c$  and  $V_d$  due to gust are encapsulated within the bounds of the flight envelope. However for the  $-\Delta n$  critical loads, only  $V_d$  is contained by the flight envelope as  $V_c$  extends past NLAA 1 condition. Hence when performing analysis for the critical load conditions applied to the aircraft wing, the gust critical loads for  $-\Delta n$  at cruise speed will be evaluated superseding NLAA 1 critical load condition's  $F_N$  and  $F_x$ . Final critical load conditions used to analyze the wing design are shown in Table 6 below.

|             | PHAA   | NHAA   | PLAA   | NLAA 1<br>(gust) | NHAA 2 |
|-------------|--------|--------|--------|------------------|--------|
| $\alpha$    | 25     | 20     | 1.873  | -4.225           | -2.995 |
| $n$         | 4.4    | -1.76  | 4.4    | -2.16            | -1     |
| $F_N$ [lbf] | 14,080 | -5,632 | 14,080 | -6,920           | -3,200 |
| $F_x$ [lbf] | -4,199 | -1,322 | 92     | -1,488           | -7.7   |

|                |      |      |        |      |        |
|----------------|------|------|--------|------|--------|
| $M_y$ [lbf ft] | -233 | -115 | -8,554 | -135 | -5,978 |
|----------------|------|------|--------|------|--------|

**Table 6. Summary of Flight Envelope Critical Load Conditions**

#### IV. WING ANALYSIS PSEUDOCODE

With the critical loads defined in the flight envelope boundary, the wing design parameters can be curated in accommodation for these conditions. To reach an optimal wing design given the fixed wing framework, MATLAB was used to iterate and simulate several combinations of variable wing parameters.

MATLAB was used to converge on an optimal wing design, taking an iterative Monte Carlo approach. As shown in Figure 11, the loads from each critical load condition (PHAA, NHAA, PLAA, NLAA) are first declared. Then, through 1000 iterations per run, the wing's input parameters are randomly generated and used to define the weight of the entire wing. These generated inputs are consequently used to compute the stresses applied in each stringer and panel (via given "wingAnalysis" script) in tandem with the critical stresses to analyze wing failure modes: buckling, yield, and wing divergence. At the end of the MATLAB script, these failure modes are assessed to verify whether the wing design iteration passes or fails; each iteration is saved in either "goodWings" or "badWings" arrays to be observed after the script run is finished. This procedure is highlighted in successive sections.

```

call criticalLoads
for i=1:1000 %1000 random wings
    call setGeometry
    call computeWeight
    call wingAnalysis
    call computeStresses
    call criticalStresses
    call failureCheck
    call saveWing
end

```

**Figure 11. Wing Analysis Pseudocode Structure**

## V. STRESSES

### A. Load Distributions

The aircraft wing in this project is thought of as a cantilever beam: one fixed end (attached to the fuselage) and one free end (wing tip). The loads imparted on the wing due to lift and drag will impose both shear and bending loads across the span of the wing. In the context of the NACA 2412 wing analysis, the load distributions are distinguished between lift ( $F_z$ ), drag ( $F_x$ ), and pitching moment ( $M_y$ ), and weight distributions.

The lift distribution analysis is assumed to be defined by the average between uniform and elliptical load distributions (numerically integrated) as shown in Figure 12. The drag distribution analysis is assumed to be defined by a uniform profile with an additional drag load distribution toward the tip of the wing; a 25% higher drag profile applied to the outer 20% of the wing. The pitching moment is assumed to be uniform across the wing span as shown in Figure 13. Lastly, the weight of the wing is assumed to be uniformly distributed across the wing span as shown in Figure 14.

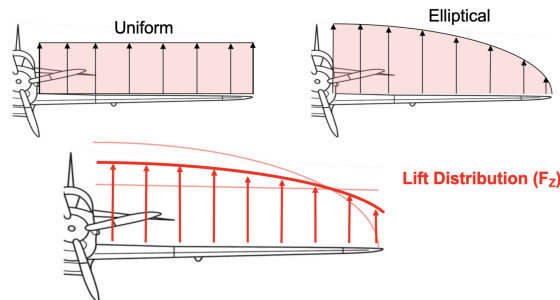


**Figure 12. Lift Distribution**

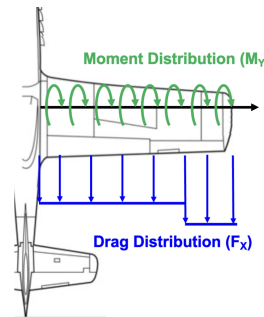


**Figure 13. Drag and Pitching Moment Distribution**

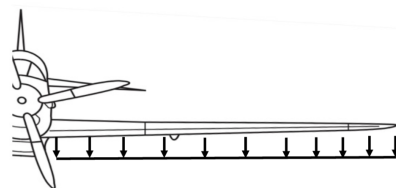


**Figure 14. Weight Distribution**

### B. Buckling Applied Stresses - Stringers and Spar Caps

Distributive  $F_N$  and  $F_X$  critical loads applied in the Z and X directions lead to an imminent build up of shear and bending stress (also represented as compression/tension) along the wing span; these stresses are expressed as  $V_Z$  (Z-direction shear due to  $F_N$ ),  $V_X$  (X-direction shear due to  $F_X$ ),  $M_Z$  (moment about the Z-axis due to  $V_X$ ) and  $M_X$  (moment about the X-axis due to  $V_Z$ ).

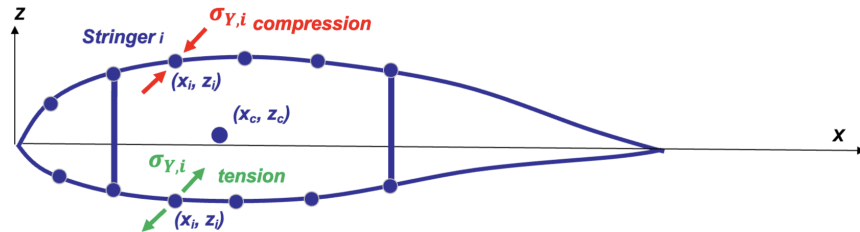


**Figure 15. NACA 2412 - Compression/Tension at Stringers**

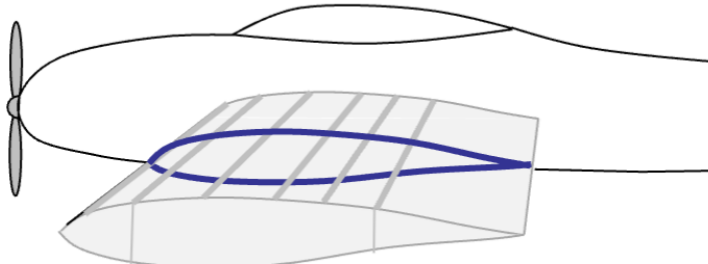


**Figure 16. Illustrates Airfoil Cross-section**

Depending on the direction of these critical loads and location relative to the centroid of each cross-section along the wing span, the stringers of the wing will experience a difference in compressive/tensile stresses directly impacted by  $M_Z$  and  $M_X$ . The effects of  $M_Z$  and  $M_X$  linearly combine, hence the sum of their contribution to each stringer evaluates the total bending which represents the compression/tension at each stringer. The bending stresses at each stringer was solved using the following equations:

$$\sigma_{Y,i} = (x_i - x_c) \frac{I_x M_z + I_{xz} M_x}{I_x I_z - I_{xz}^2} - (z_i - z_c) \frac{I_z M_x + I_{xz} M_z}{I_x I_z - I_{xz}^2}$$

The overall wing geometry, specifically the position and area of each stringer, directly influences the moments of inertia and centroid location for the NACA 2412 airfoil. These values are calculated in the following equations and applied to the bending stress equation above:

$$x_c = \frac{\sum x_i A_i}{\sum A_i}$$

$$z_c = \frac{\sum z_i A_i}{\sum A_i}$$

$$I_x = \sum A_i (z_i - z_c)^2$$

$$I_z = \sum A_i (x_i - x_c)^2$$

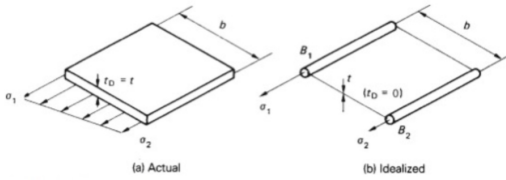
$$I_{xz} = \sum A_i (x_i - x_c)(z_i - z_c)$$

When calculating the centroid of the airfoil, it was assumed that the webs/panels can be neglected since they are relatively thin. This simplifies the process for defining the moments of inertia, centroid, and bending stresses at each cross-section of the wing. As a way to simply incorporate the contribution of the panels ability to alleviate the applied stresses, an “equivalent” area is added to the surrounding stringers of each panel: Panel Idealization.

The Panel Idealization method references T.H.G. Megson’s Principle of Structural Idealization. Structural Idealization references the thickness of the panels and the compressive/tensile stresses of the surrounding stringers to determine the appending area of those respective stringers, encapsulated in Figure 17.

*From Megson:*

*Find area of equivalent stringer,  $B_1$  by equating the moments due to the stress distribution (taken about stringer  $B_2$ )*



$$\int_0^b \left[ \sigma_2 t_D + \frac{t_D(\sigma_1 - \sigma_2)}{b} l \right] l dl = \sigma_1 B_1 b$$

$$\frac{\sigma_2 t_D b^2}{2} + \frac{t_D(\sigma_1 - \sigma_2)b^2}{3} = \sigma_1 B_1 b$$

Solving for  $B_1$ :  $B_1 = \frac{t_D b}{6} \left( 2 + \frac{\sigma_2}{\sigma_1} \right)$

Similarly for  $B_2$ :  $B_2 = \frac{t_D b}{6} \left( 2 + \frac{\sigma_1}{\sigma_2} \right)$

**Figure 17. Illustration of Megson’s Structural Idealization**

In the context of this wing analysis, the Megson Structural Idealization equations will be modified to emphasize the Z position of the surrounding stringers rather than the stress applied. This refined area will determine the modified moments of inertia, centroid, and bending stress values. This method is ideal since the modified moments of inertia are required to determine the modified and alleviated bending stress values, and not the other way around. The refined equations are exhibited below:

$$B_1 = \frac{t_D b}{6} \left( 2 + \frac{(z_2 - z_c)}{(z_1 - z_c)} \right)$$

$$B_2 = \frac{t_D b}{6} \left( 2 + \frac{(z_1 - z_c)}{(z_2 - z_c)} \right)$$

Panel Idealization and bending stress analysis is performed for each spar cap. MATLAB was used to follow these methodologies and equations for all Top, Bottom, Nose Top, Nose Bottom

Stringers, and Spar Caps. The “wingAnalysis” MATLAB script calculates the unit bending stresses at each stringer which is scaled up by the magnitudes of  $M_z$  and  $M_x$  influenced by position along the wing span to indicate the actual applied bending stress.

### C. Buckling Applied Stresses - Webs

The stress analysis for the stringers are meant to convey the structural rigidity of the wing as a whole. Although the panels were neglected for the stringer/structural analysis, the stress applied at each web must be analyzed to prevent failure at the individual component scale during operation. The webs in consideration include: top panels, bottom panels, nose top panels, nose bottom panels, front spar, and rear spar. As shown in Figure 18, *shear* and *bending* stresses will be determined for the nose panel front spar, and rear spar whereas the *shear* and *compression* stresses will be determined for the top, bottom, nose top, and nose bottom panels.

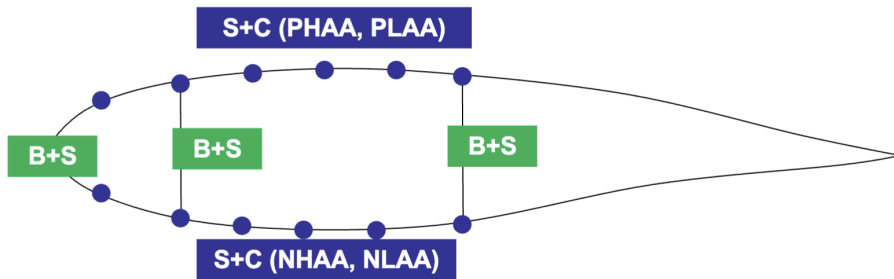


**Figure 18. Types of Stress Analysis on Distinct Webs/Spars**

#### A. Shear Buckling Stress

The shear buckling stresses imposed on aircraft webs is principally solved by finding the total shear flow per web, i.e. the longitudinal shear force transmitted per unit length across the web, at each panel (by cell) and dividing that total shear flow by the thickness. The process to calculate the shear flow for each web is conveyed below:

1. Solve for shear flow webs due to pure shear/bending, no twist,  $q_{1s}$  and  $q_{2s}$  using twist equations for a two cell box beam:

$$\theta_1 = \frac{q_1}{A_1} \sum \frac{\Delta S_i}{t_i} - \frac{q_2}{A_1} \left( \frac{\Delta S}{t} \right)_{interior}$$

$$\theta_1 = \theta_2 = \frac{q_2}{A_2} \sum \frac{\Delta S_i}{t_i} - \frac{q_1}{A_2} \left( \frac{\Delta S}{t} \right)_{interior}$$

2. Solve for shear center using the torque equations

$$T = \Sigma 2Aq = Vx$$

3. Solve for shear flow of webs due to twist using the torque relative to the shear center & the actual applied load and the twist equation
4. Solve for total shear flows for all webs using the follow equation:

$$q_{tot} = q_s + q_t + q'$$

The “wingAnalysis” MATLAB script follows this process, for each cross-sections along the wing span, to determine the unit shear flows for all webs. The actual, applied shear flows for each web is solved by multiplying the unit shear flow with their respective shear forces or pitching moment and summing all load cases. An example is depicted in Figure 19:

**Example: If at a specific cross-section  
 $V_z = 1000, V_x = 500, M_y = 200$**

$$q_{i,tot} = 1000 \times q_{tot,Vz=1} + 500 \times q_{tot,Vx=1} + 200 \times q_{tot,My=1}$$

**Figure 19. Example for Deriving  $q_{i,tot}$**

The shear stress for a web at each cross-section is then determined by dividing the total shear flow of the web by the web thickness. Ultimately, the shear stress of the individual web is assumed to be the average of the cross-sectional shear flows sandwiching that web, indicated in Figure 20.

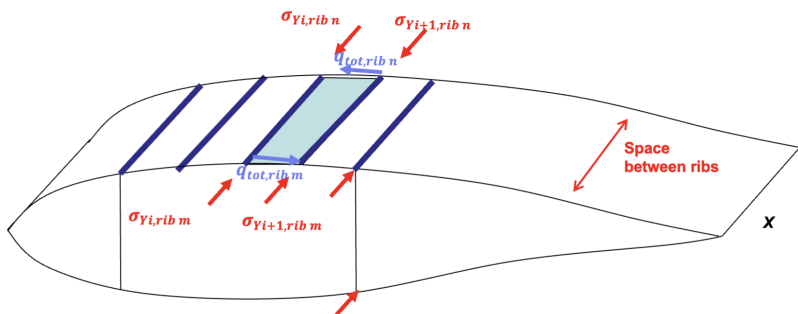


**Figure 20. Shear and Compressive Stresses at Cross-sections**

### B. Compressive Buckling Stress

For this project, the compressive buckling stress applied to each panel is assumed to be the average between the stringers and/or spar caps surrounding them. In Figure 20, it would be the average between the four compressive stresses surrounding the highlighted panel.

### C. Bending Buckling Stress

Due to very high load values for lift (as a result of  $V_z$  derived  $M_x$ ), relative to drag, the bending stresses of the nose, front spar, and rear spar must be analyzed for stress; bending stresses are invoked by lift since  $M_x$  creates distinct compression and tension zones about the Nose, Front Spar, and Rear Spar between the top-side and bottom-side panels. The bending stresses of these wing components are solved by averaging the absolute values of the compressive and tensile stresses of the stringers or spar caps sandwiching the nose, front spar, and rear spar.

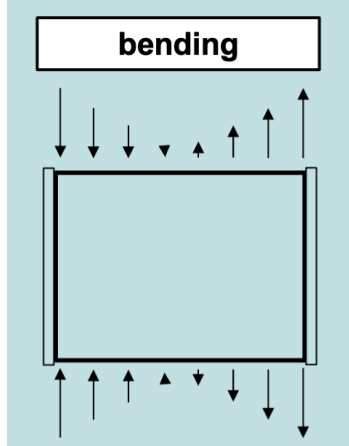


**Figure 21. Bending Stress About Nose, Front Spar, and Rear Spar**

## VI. CRITICAL STRESSES

### A. Buckling Failure Stress - Stringers and Spar Caps

The critical stress for column buckling must be assessed to ensure the stringers and spar caps do not fail under compressive stresses along the wing span. In the event that critical buckling stresses are exceeded, corresponding stringers and spar caps will undergo structural deformation. The critical stresses for each stringer/spar cap of the wing is determined using the Euler column formula which assumes pinned end conditions:

$$P_{cr} = \frac{\pi^2 EI}{L^2}$$

The column length used in the Euler column buckling equation varies depending on the end constraints used for the stringers and spar caps. Figure 22 shows the different column effective length factors (K). Pinned end constraints allow members to rotate around a given end but restricts lateral and vertical translation. Fixed end constraints does not permit rotation or any form of translation. Stringers are not exactly pinned ( $K=1$ ) but rather fastened or fixed ( $K=0.5$ ) to ribs chords generally improving the critical buckling stress threshold. Realistically, these fastened end cannot be considered fully fixed to ribs. Hence, the column effective length factor  $K=0.7$  is assumed when solving for these stringer and spar cap critical buckling stress values:

$$P_{cr} = \frac{\pi^2 EI}{KL^2}$$

*Note:  $I = I_{xx}$  is applied to critical buckling stress equations corresponding to the randomly selected stringer shape when generating wing geometry inputs. Panel idealization modifications are not applied to stringer moments of inertia.*

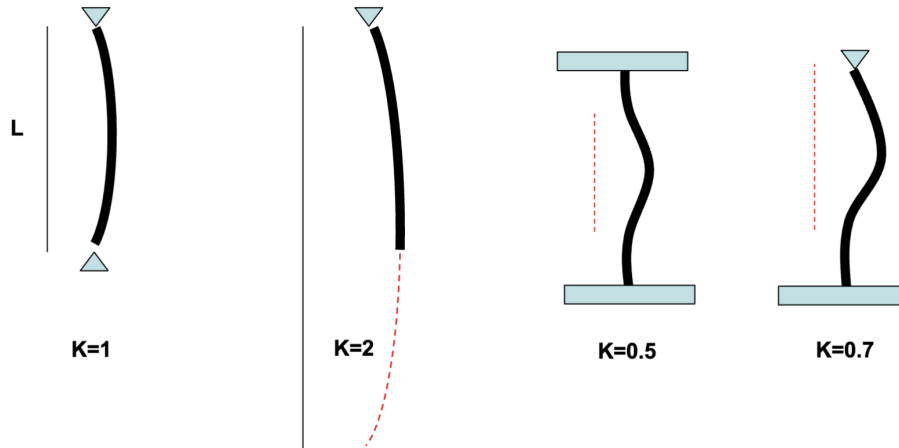


**Figure 22. Column Effective Length Factors**

All stringers and spar caps share the same geometry: length, shape, area, moments of inertia. Therefore, all stringers and spar caps share the same critical buckling stress values at each cross-section along the wing span.

### B. Buckling Failure Stress - Webs

The critical stresses for each web is assessed for buckling due to shear, compression, and/or bending. As aforementioned in the “Stresses” section, *shear* and *bending* stresses were determined for the nose panel front spar, and rear spar whereas the *shear* and *compression* stresses were determined for the top, bottom, nose top, and nose bottom panels, shown in Figure 18. The same type of critical stresses will be calculated for respective webs using the flat panel buckling equation:

$$\sigma_{CR} = \frac{k\pi^2 E}{12(1-\nu^2)} \left(\frac{t}{b}\right)^2$$

The buckling coefficient (k) used in the flat panel buckling equation changes depending on the type of critical stress. Figure 23 depicts the graphs used to determine these different buckling coefficients. It is assumed that the (a/b) values will be relatively high for each stress type; where “a” is the web length and “b” is the web width. For that reason, the buckling coefficient will be drawn where the curves begin to plateau. Using the same end condition described made for stringers, it will be assumed the buckling coefficient can be drawn from the average between the unloaded edges clamped and unloaded edges pinned. The buckling coefficients are used for the following buckling stress types:

- $k_{\text{shear}} = 9$
- $k_{\text{compression}} = 6$
- $k_{\text{bending}} = 34$

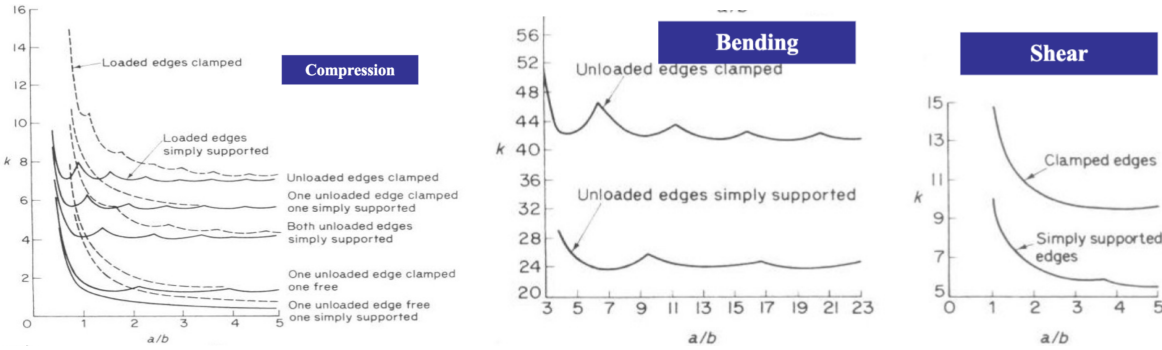


Figure 23. Buckling Coefficient Curves

### C. Curved Panel - Panels

Curved panels have a higher critical buckling stress values that increases as the radial feature decreases. Throughout the geometry of the airfoil, all top and bottom panels are known to be curved since they outline the NACA 2412 profile. To qualify the curved feature's contribution for each panel, the following equation can be solved:

$$\frac{\sigma_{CR}}{E} = 9\left(\frac{t}{R}\right)^{1.6} + 0.16\left(\frac{t}{L}\right)^{1.2}, \text{ for } 500 < \frac{R}{t} < 3000$$

$$\sigma_{CR} = 0.3E\frac{t}{R}, \text{ for } \frac{R}{t} > 3000$$

The radius for each panel is found by using the following equation, where  $\Delta\theta$  is the change in angle between the start and end of each panel, exemplified in Figures 24 and 25:

$$R = \frac{\Delta s}{\Delta\theta}$$

The critical buckling stress values calculated above for each panel on the wing were appended to the critical buckling stress values found with the flat panel buckling equation, from “Buckling Failure Stress - Webs” subsection, for shear, compression, and bending. Spars are not included in this analysis since they are completely flat.

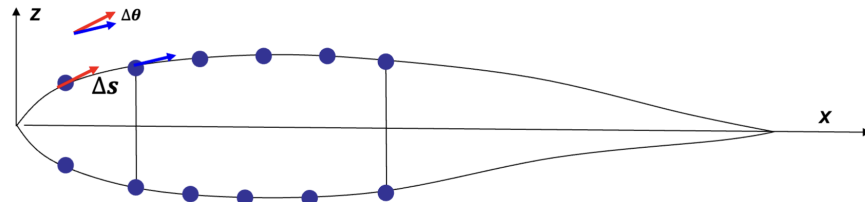
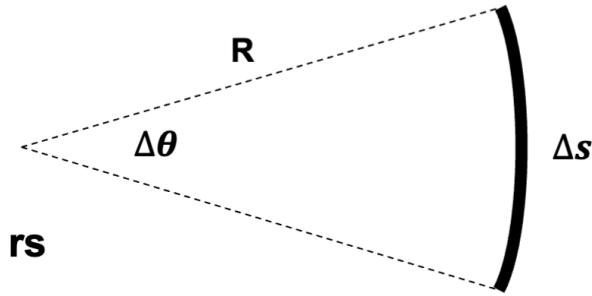


Figure 24. Method to Obtain  $\Delta\theta$



**Figure 25. Method to Obtain Radius for Panels**

## VII. FAILURE CRITERIA

To ensure aircraft wing integrity during operational use, analysis was performed on each wing iteration for the following failure modes: buckling, yield, and wing divergence. For each MATLAB wing design iteration, the script runs through this failure criteria checklist to decide the pass/fail status for each randomly generated wing geometry. For all failure mode analyses, an additional 50% safety margin must be considered i.e. factor of safety (FOS) of 1.5.

### A. Buckling Failure Criteria - Stringers and Spar Caps

The applied bending stresses and critical buckling stresses results calculated for all stringers can be directly compared to one another to determine the failure ratio ( $R$ ). This ratio is referenced to decide whether a wing geometry passes or fails the buckling failure checkbox. Per wing design requirements, an additional 50% safety margin must also be considered:

$$R = \frac{(1.5)(\text{applied bending stress})}{(\text{stringer critical stress})} = \frac{\sigma_b}{\sigma_{CR}}$$

If the failure ratio exceeds 1, the respective stringer fails and hence the wing design iteration fails. The same analysis is performed for spar caps since they share the same features as all stringers.

### B. Buckling Failure Criteria - Webs

The buckling failure analysis for each web is different compared to the buckling failure analysis for all stringers. Since different types of webs experience either a combination of *shear and compression* (top, bottom, nose top, and nose bottom panels) or of *bending and shear* (nose, front spar, and rear spar) illustrated in Figure 18, their respective failure criteria changes. The failure criteria for both distinct combinations of stress are described below:

$$\begin{aligned} & R_s^{1.5} + R_c, \quad \text{Shear and Compression (S+C)} \\ & R_b^2 + R_s^2, \quad \text{Bending and Shear (B+C)} \end{aligned}$$

If failure ratio summations for web stress combination exceed 1, the respective web fails and hence the wing design iteration fails. The applied stresses and critical buckling stresses results

calculated for each web can be directly compared to one another to determine shear buckling failure ratio ( $R_s$ ), compressive buckling failure ratio ( $R_c$ ), bending buckling failure ratio ( $R_b$ ). Per wing design requirements, an additional 50% safety margin must also be considered.

$$R_s = \frac{(1.5)(\text{applied shear stress})}{(\text{stringer critical stress})} = \frac{\sigma_s}{\sigma_{CR,S}}$$

$$R_c = \frac{(1.5)(\text{applied compressive stress})}{(\text{stringer critical stress})} = \frac{\sigma_c}{\sigma_{CR,C}}$$

$$R_b = \frac{(1.5)(\text{applied bending stress})}{(\text{stringer critical stress})} = \frac{\sigma_b}{\sigma_{CR,B}}$$

### C. Yield Failure Criteria

The material used for this wing design is randomly chosen between Aluminum 7075-T6, 2024-T4, and 2014-T6 due to their high strength to weight ratio. For each wing design and analysis iteration, it is critical that the von Mises stress yield criteria does not exceed the yield strength, or young's modulus ( $E$ ), of the selected aluminum alloy. The von Mises stress analysis will be performed on all top and bottom panels which encompass the entire wing. The von Mises stress can be found using the following equation:

$$\sigma_v = \sqrt{\frac{\sigma_1^2 + \sigma_2^2 + (\sigma_1 - \sigma_2)^2}{2}}$$

The principal stresses ( $\sigma_1$  and  $\sigma_2$ ) used to calculate the von Mises stress for each panel are determined using Mohr's circle analysis, Figure 26, by rotating corresponding compressive and shear stresses using the following equation:

$$\sigma_1, \sigma_2 = \frac{\sigma_y}{2} \pm \sqrt{\left(\frac{\sigma_y}{2}\right)^2 + \tau_{xz}^2}$$

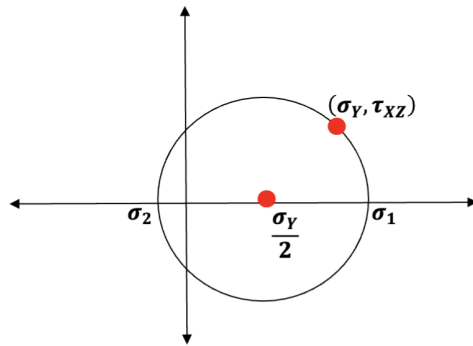


**Figure 26. Mohr's Circle Analysis with Panel Stresses**

Per wing design requirements, an additional 50% safety margin must also be considered. If the yield failure ratio ( $R_Y$ ) exceeds 1, the respective panels fail and hence the wing design iteration fails. The yield failure ratio is defined below:

$$R_Y = \frac{(1.5)(\text{von Mises Stress})}{(\text{Material Yield Strength})} = \frac{\sigma_v}{\sigma_y}$$

#### D. Wing Divergence

Lastly, the wing divergence for the wing design structure as a whole must be considered. The wing divergence is the aero-elastic effect when twisting moments caused by large lift/drag forces overpower the torsional rigidity of the wing. This failure criteria is indicated by the wing divergence velocity. The wing divergence velocity can be determined using the following equation:

$$V_{divergence} = \sqrt{\frac{\pi^2 G J}{2 \rho C_{L,a} e c^2 \left(\frac{b}{2}\right)^2}}$$

Where,

- G, material shear modulus
- $J = I_{XX} + I_{ZZ}$ , airfoil torsional constant (derived from “wingAnalysis” script per iteration)
- $C_{L,a} = 4.1242$ , lift coefficient & angle of attack slope (derived from XFOIL)
- $\rho = 23.77 \times 10^{-4} \frac{\text{slug ft}}{\text{s}^2}$ , air density at sea level
- e, nondimensional distance between the position of applied load and shear center
- c = 5 ft, chord length
- b = 34 ft, full wing span

If the wing divergence velocity threshold well exceeds the defined dive speed of the aircraft, the wing avoids this potential failure mode and the wing design iteration passes.

## VIII. WING OPTIMIZATION

Using the developed code exemplified in the “Wing Analysis Pseudocode” section, the Monte Carlo technique was used to fully define weight-efficient wing design parameters for it’s given function and fixed framework. Since there are four distinctions of failure criteria (stringer buckling, web buckling, yield, and wing divergence failure), the structured Monte Carlo method applied was to iterate ranges of different wing design parameters and succeed with one failure criteria successively including the next. The strategy behind this method is to have a high wing design success rate in the first failure criteria analysis and proportionally dilute this success rate as more failure criteria is tested. This method was performed in the following order:

1. Stringer and spar cap buckling failure check - ~80% success rate
2. Include web buckling failure check - ~60 % success rate
3. Include yielding failure check - ~40% sucess rate
4. Include wing divergence failure check - ~20% success rate

This structured Monte Carlo approach is efficient and effective such that it guarantees the functionality of the wing from beginning to end while consistently converging on an optimal wing design range parameters; this also saves time since debugging occurs every step of the way (rather than testing and debugging larger scripts or combinations of scripts). It prompts educated guessing and learning of what parameters and/or combinations of parameters affect each failure

criteria. Logistically per failure check, if the iteration success rate is lower than the desired success rate, corresponding design range parameters are changed to increase this success rate. If the iteration success rate is higher than than the desired success rate, corresponding design range parameters are changed to dilute this success rate in favor of reducing wing weight. Prompt changes are made in consideration of effects prior failure checks.

Since this process begins at such a high success rate, most wing components will be over-built. Ranges will have to change lower and lower to match desired success rates. At this point, iterations are performed (in favor of minimizing weight) until the script converges on an optimal combination of wing design parameters. MATLAB data results for structured Monte Carlo approach is demonstrated below.

#### Stringer and Spar Cap Buckling Failure Check (~80%)

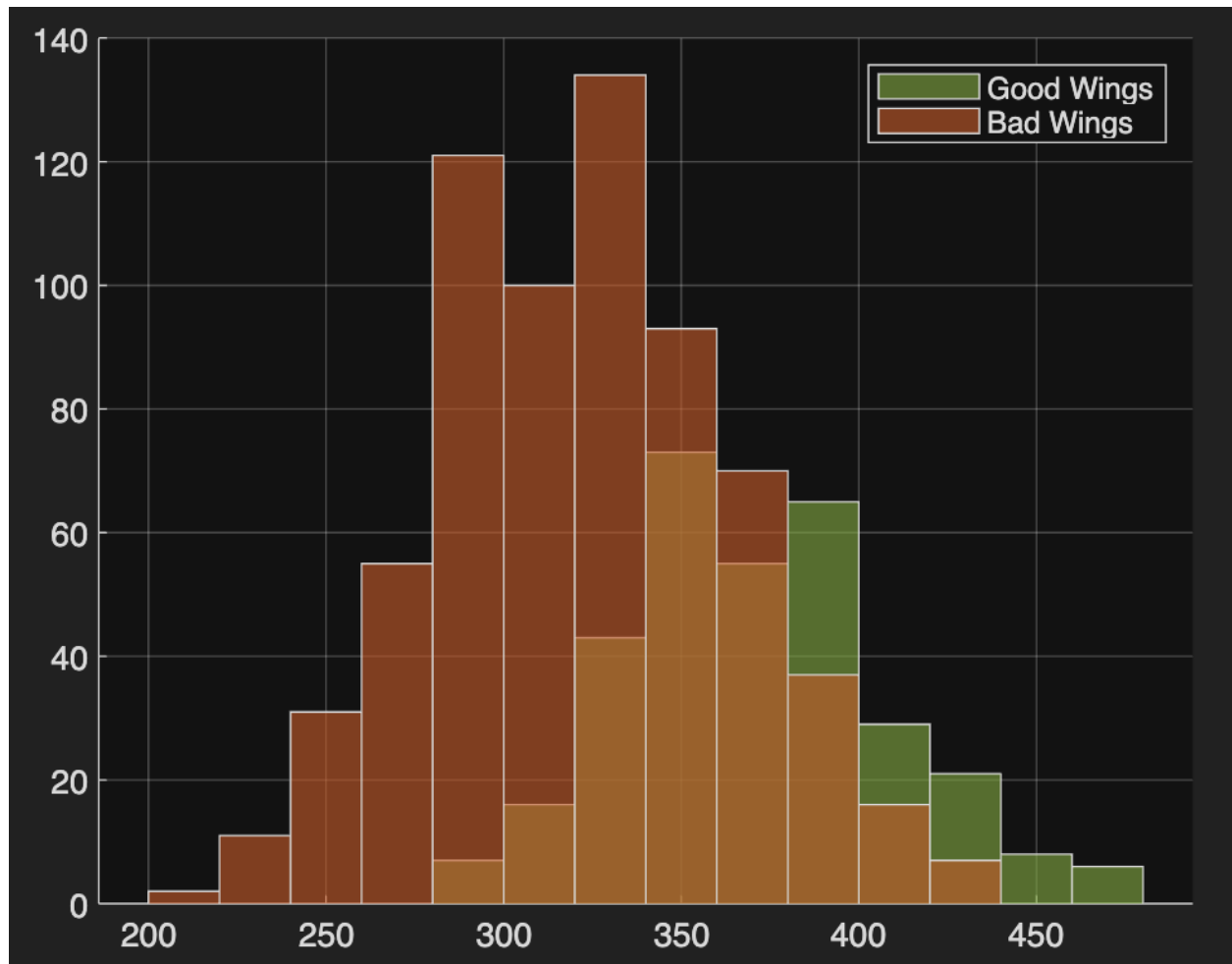


**Figure 27. Histogram - Initial Stringer & Spar Cap Buckling Failure Check**

Success rate: 51.1%

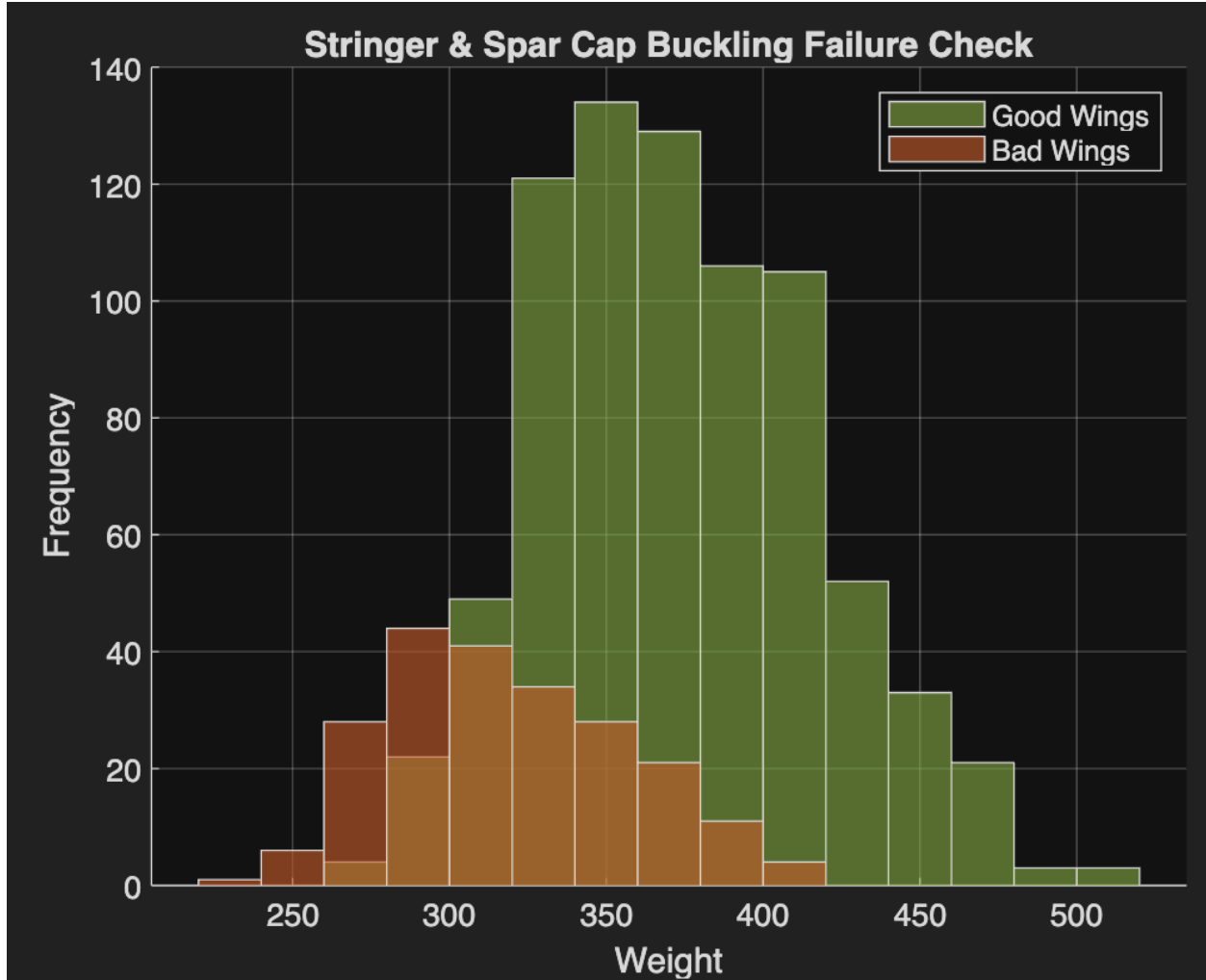


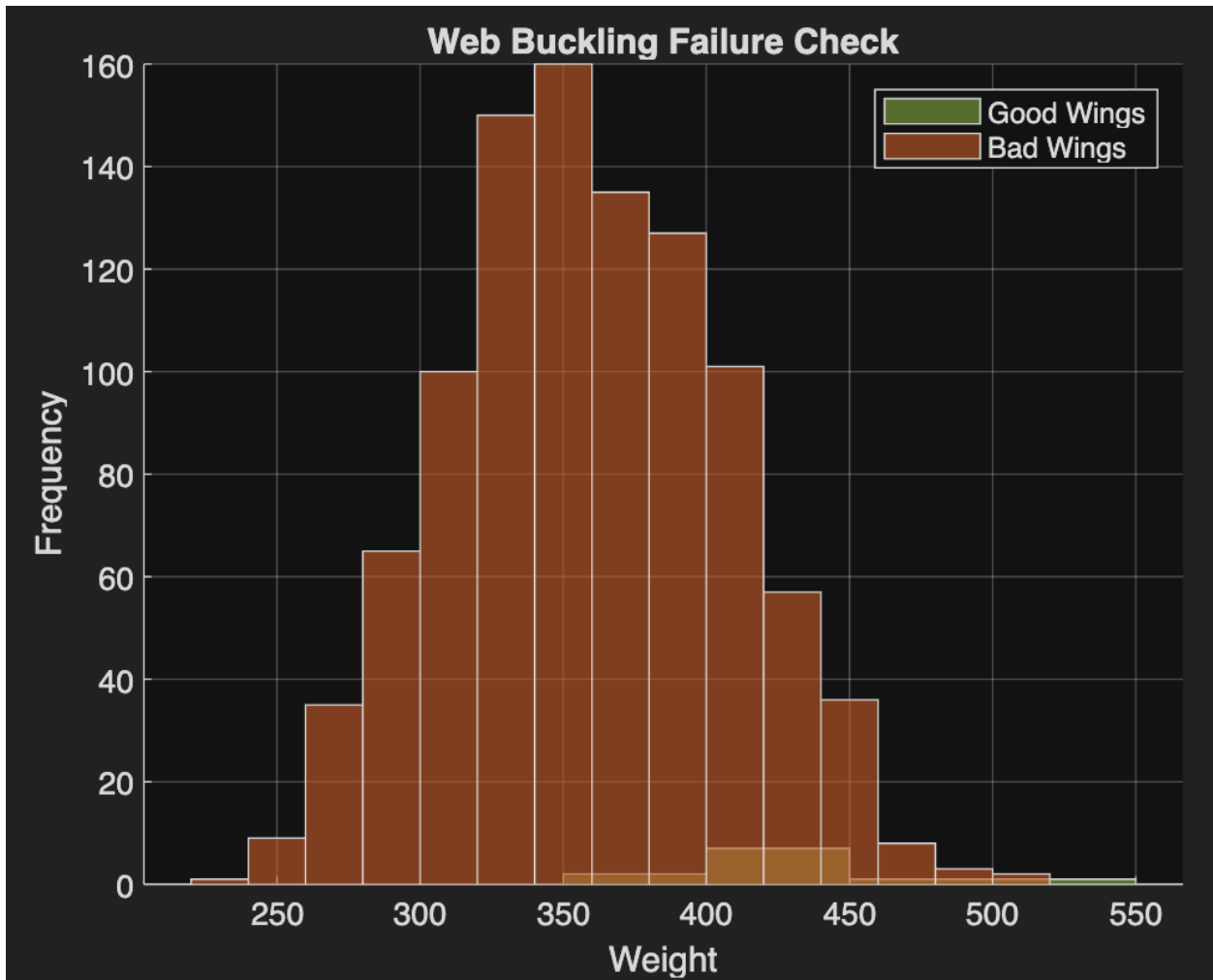
**Figure 28. Histogram - Final Stringer & Spar Cap Buckling Failure Check**

Success rate: 78.2%

Beginning with stringer and spar cap buckling failure check, the initial success rate with given wing parameters resulted in a 51.1% success rate. The final success rate for this step came out to be 78.2%. In order to increase this rate, the modified Euler column buckling equation was referenced.

$$P_{cr} = \frac{\pi^2 EI}{KL^2}$$

Logically for this failure criteria, increasing the critical buckling stress value for the stringers and spar caps leads to an increase in the success rate of each iteration check. Therefore, the parameters that can be changed include the length of each stringer as well as the moment of inertia. Promptly, the number of ribs were increased to shorten the wing stringers and Z-shaped stringers and spar caps with a higher area and moment of inertia were included until an ~80% was achieved; to maintain parameter range, Z-shaped stringers and spar caps with a lower area and moment of inertia were removed.

Web Buckling Failure Check (~60%)

**Figure 29. Histogram - Initial Web Buckling Failure Check**

Success rate: 1.1%

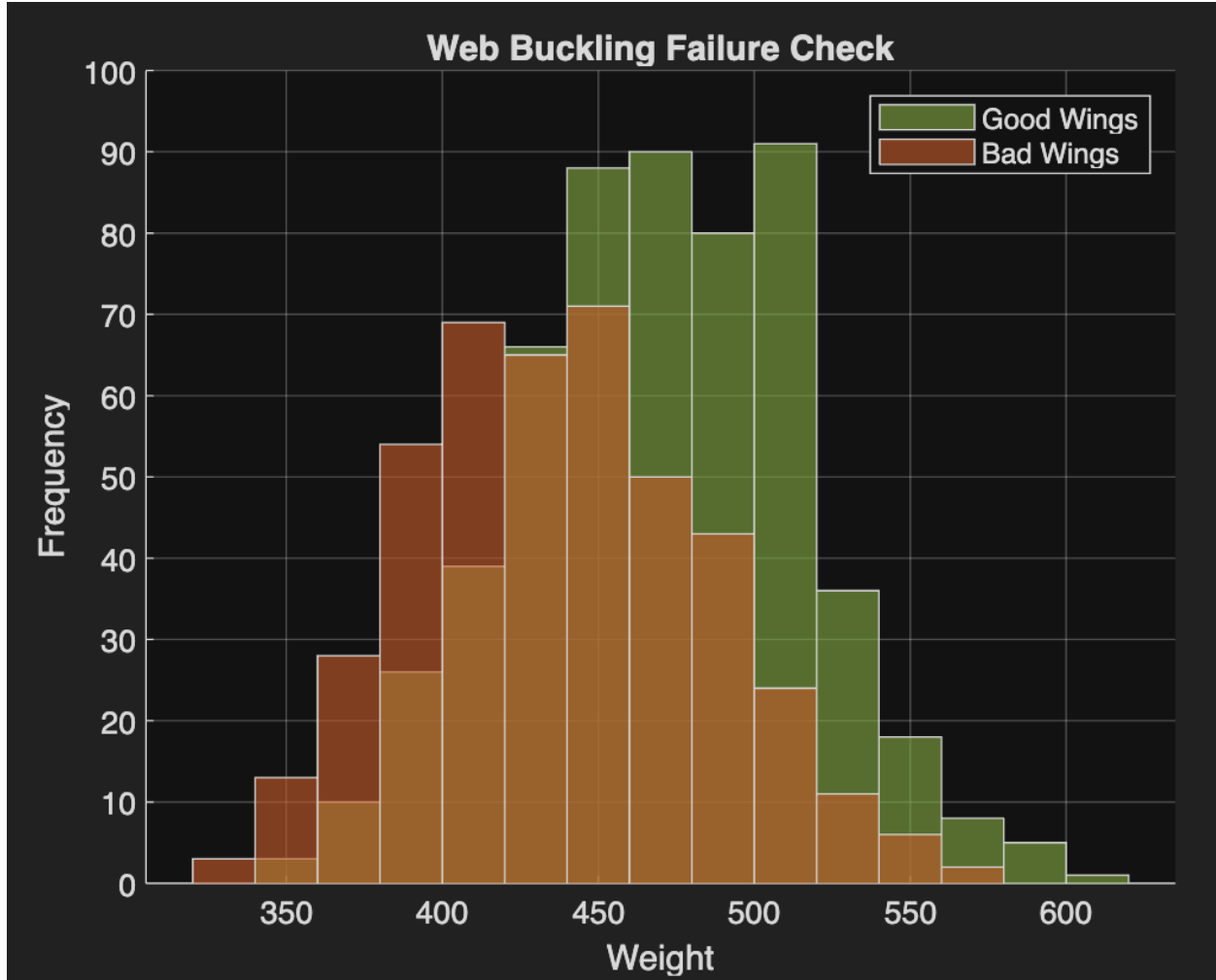


**Figure 30. Histogram - Final Web Buckling Failure Check**

Success rate: 56.1%

The initial success rate for the web buckling failure check resulted in a 1.1% success rate. The final success rate for this step came out to be 56.1%. In order to increase this rate, the flat panel buckling and curved panel critical stress equations were referenced again.

$$\sigma_{CR} = \frac{k\pi^2 E}{12(1-\nu^2)} \left(\frac{t}{b}\right)^2$$

$$\frac{\sigma_{CR}}{E} = 9\left(\frac{t}{R}\right)^{1.6} + 0.16\left(\frac{t}{L}\right)^{1.2}, \text{ for } 500 < \frac{R}{t} < 3000$$

$$\sigma_{CR} = 0.3E \frac{t}{R}, \text{ for } \frac{R}{t} > 3000$$

Similarly to the stringer and spar caps buckling failure check, the critical buckling stress values for the panels need to increase for the increase the success rate of each iteration check. This needs to be done without compromising the stringers and spar caps buckling failure check. As indicated in the equations above, the web thicknesses were increased and the web widths were

reduced (by increasing the number of stringers) accordingly until a success rate of ~60% was achieved.

Yielding Failure Check (~40%)

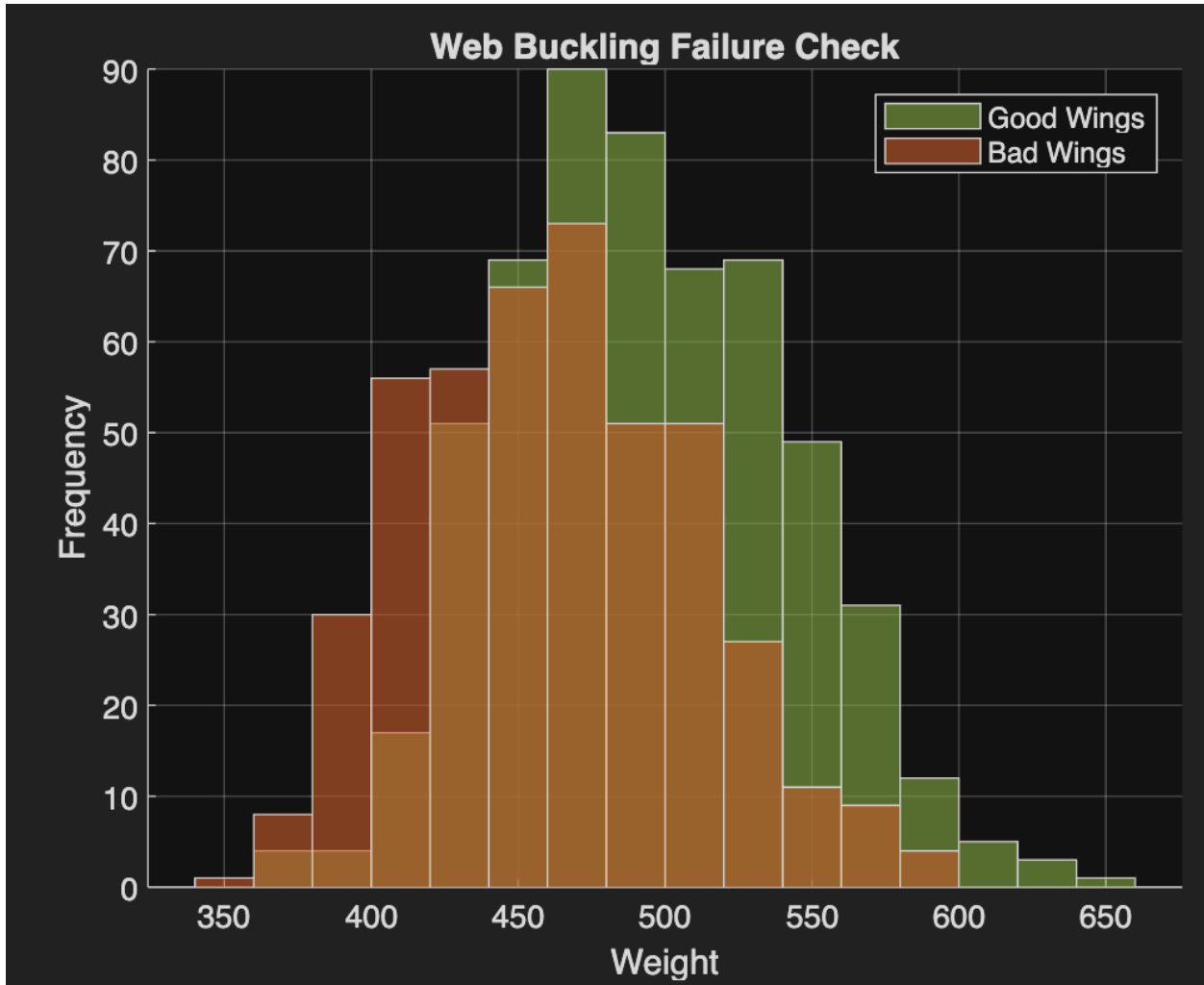


**Figure 31. Histogram - Initial Yielding Failure Check**

Success rate: 57.8%

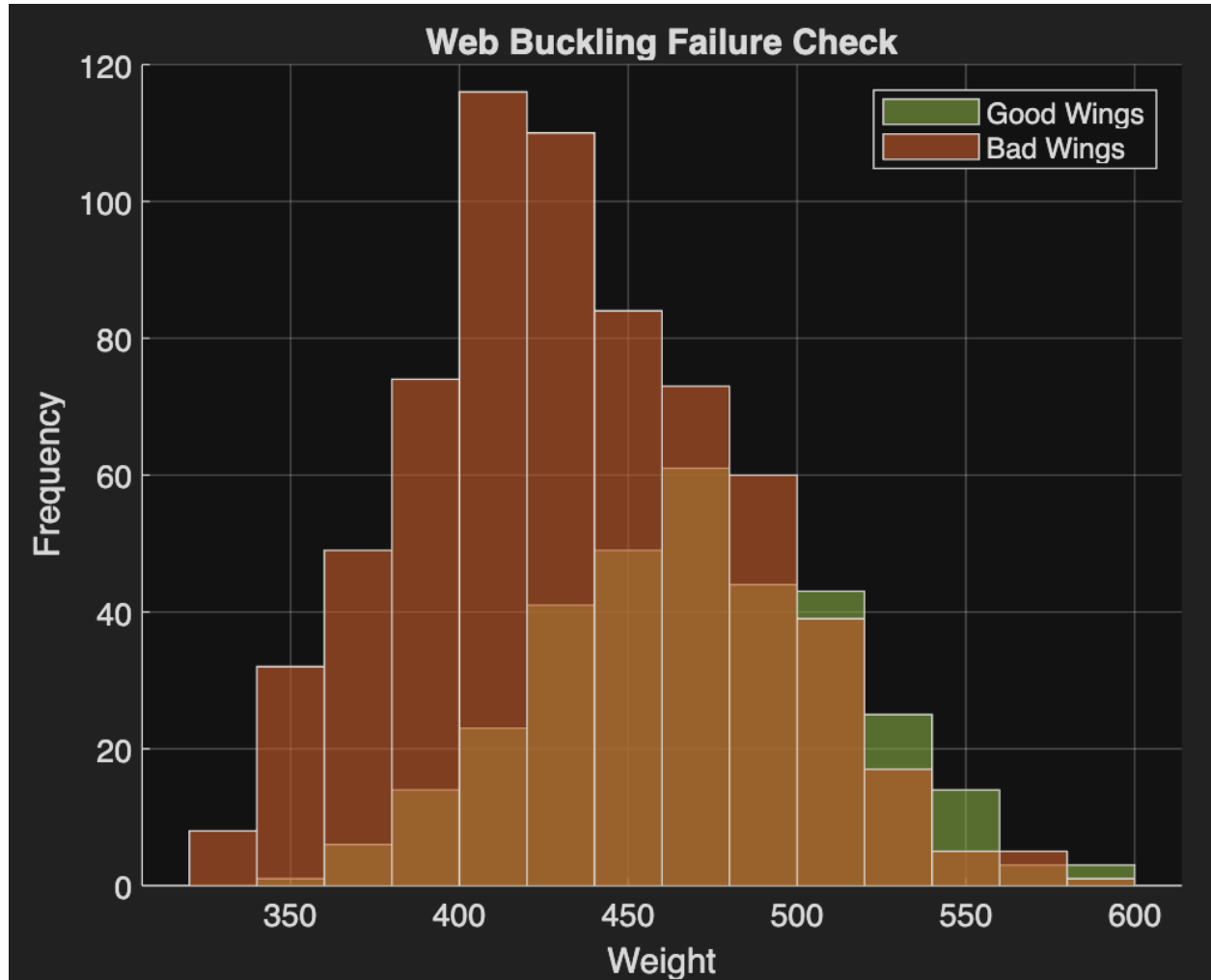


**Figure 32. Histogram - Final Yielding Failure Check**

Success rate: 38.7%

The initial success rate for the yielding failure check resulted in a 57.8% success rate, which is very similar to the final web buckling failure check success rate. This indicates that the yielding has a success rate close to 100%; hence the yielding failure check is negligible up to this point. Successively, the final yielding failure check for this step came out to be 38.7%. The same methods to decrease the success rate for stringer, spar caps, and web failure are used for this step.

Wing Divergence Buckling Failure Check (~20%)

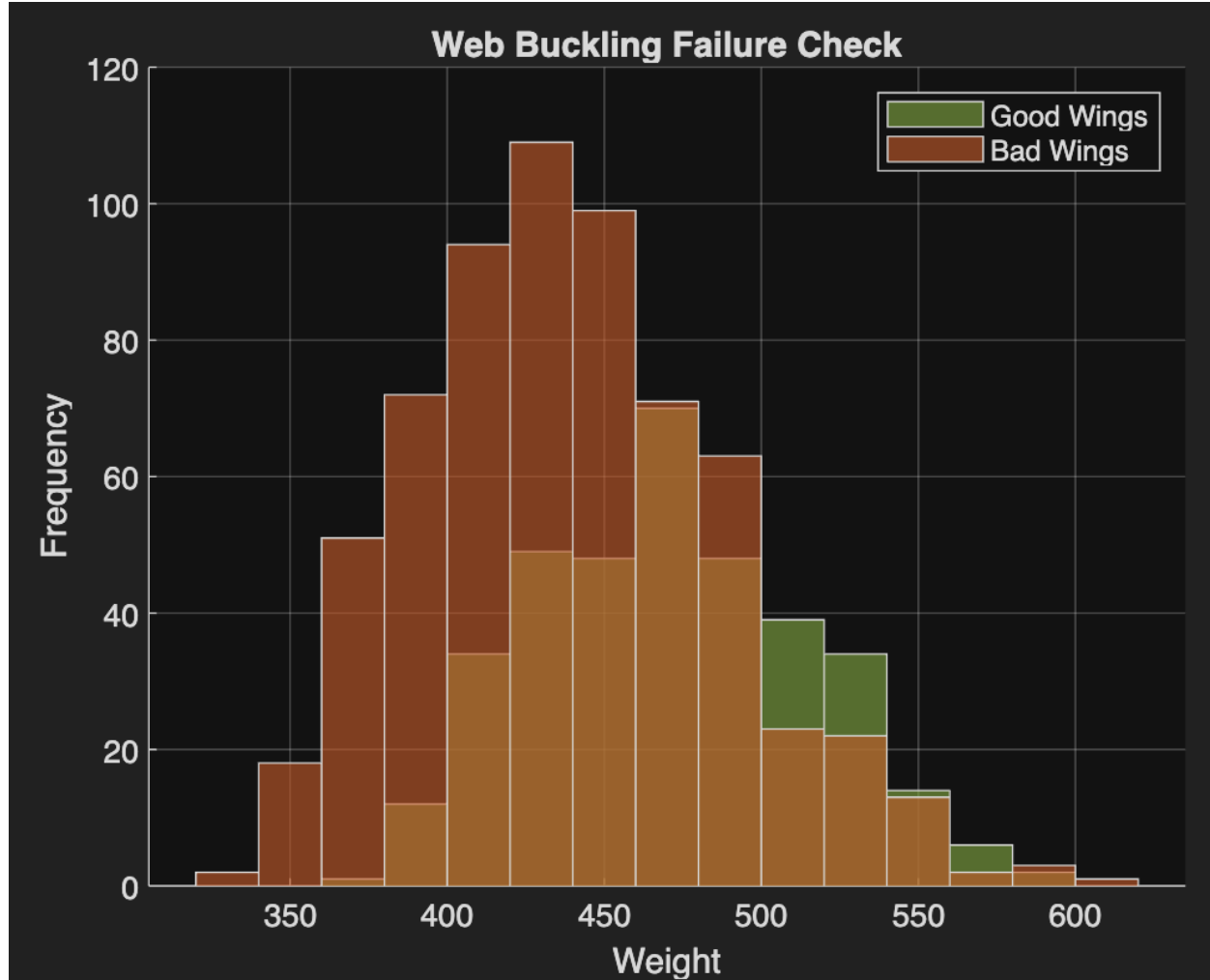
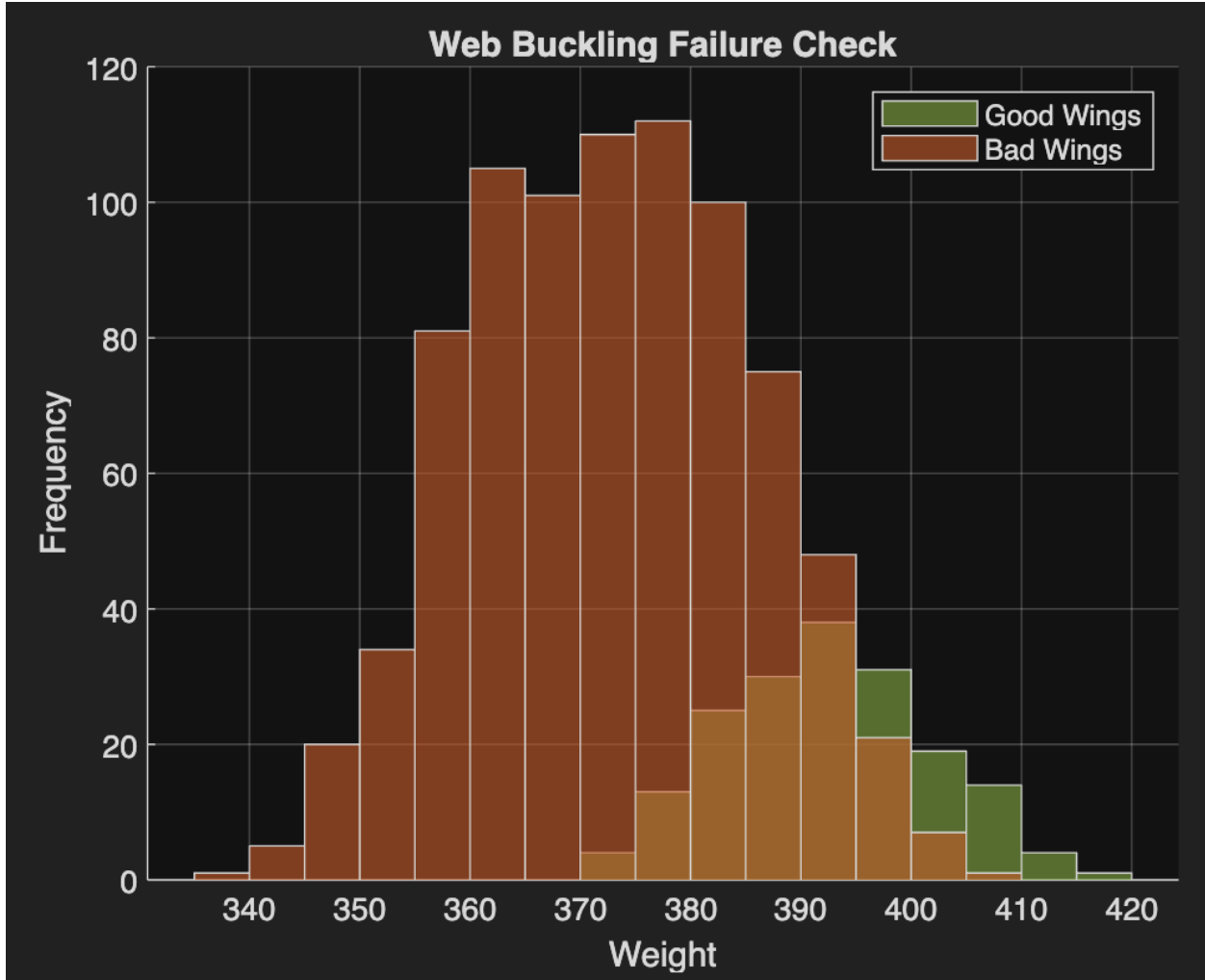


Figure 33. Histogram - Initial Wing Divergence Failure Check

Success rate: 36.2%



**Figure 34. Histogram - Final Wing Divergence Failure Check**

Success rate: 21.4%

The initial success rate for the wing divergence failure check resulted in a 36.2% success rate, which is very similar to the final yielding failure check success rate. This indicates that the wing divergence has a success rate close to 100%; hence the wing divergence failure check is negligible up to this point. Successively, the final wing divergence failure check for this step came out to be 21.4%. The same methods to decrease the success rate for stringer, spar caps, and web failure are used for this step. As shown in Figure 34, the wing parameter ranges were shifted downward indicated by the increase in lighter good/bad wings.

## IX. FINAL WING DESIGN

With all failure criterion passing with a ~20% success rate, the generated inputs for the successful wings are starting to look more consistent with one another. Before, the wing iterations were focused on wing integrity by checking all the boxes. Now, the attention is given to the weight efficiency of the working design iterations. Moving onto the final phase of the

Monte Carlo iteration process, the wing design parameters were iterated and refined based on the wing inputs of the lighter demographic of successful wings; this will inevitably start increasing the success rate of each MATLAB run. The wing design parameter ranges are narrowed per iteration until a final design is curated. Figure 35 show this sudden spike in the number of successful wings as the wing design iteration parameters begin to narrow towards more reliable inputs. The final design specifications were chosen from the lighter demographic of successful wings, plotted in Figure 36 and listed in Table 7. The plots illustrating the stress margins distributed on the top and bottom sections of the wing are shown in Figures 37-71.

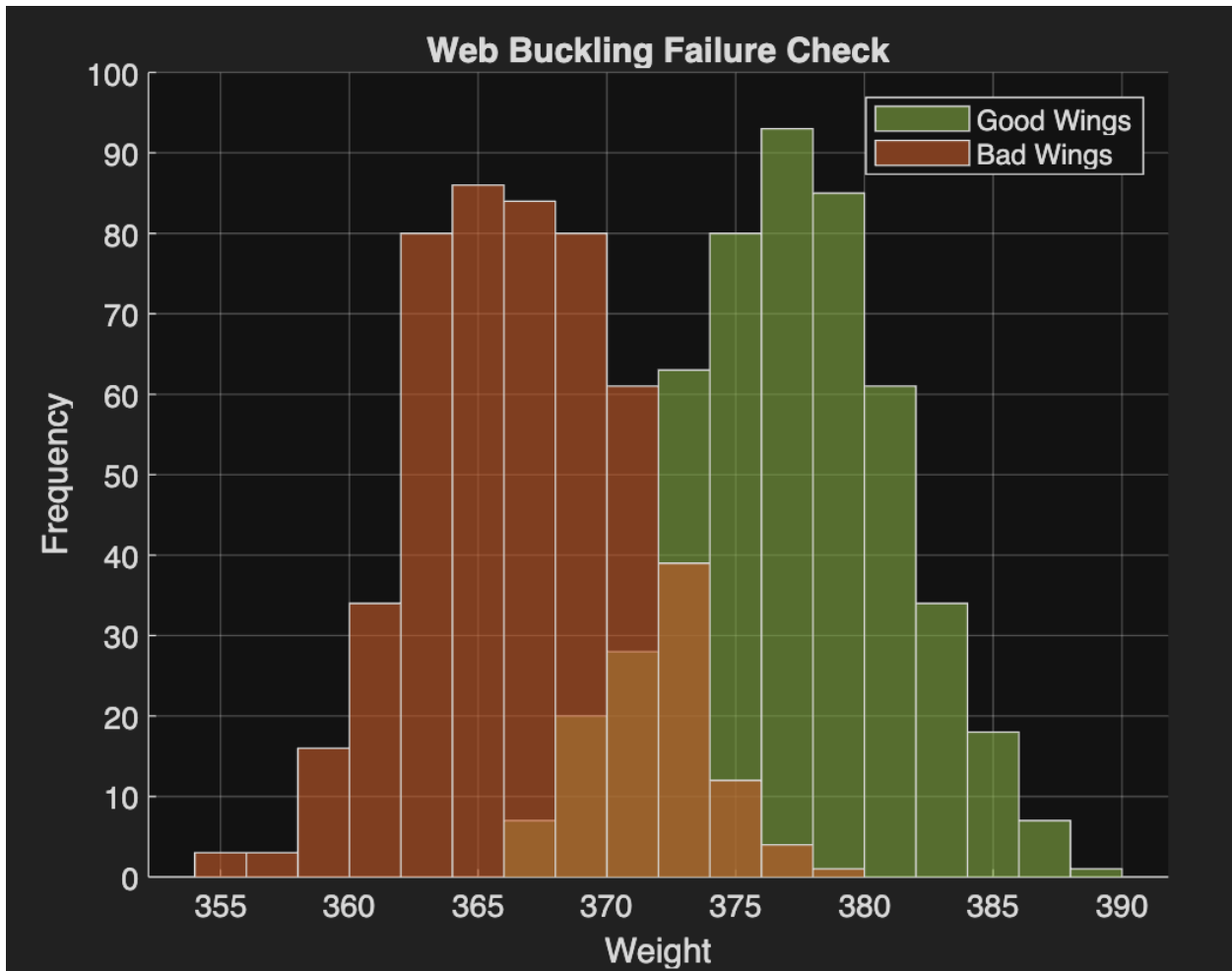
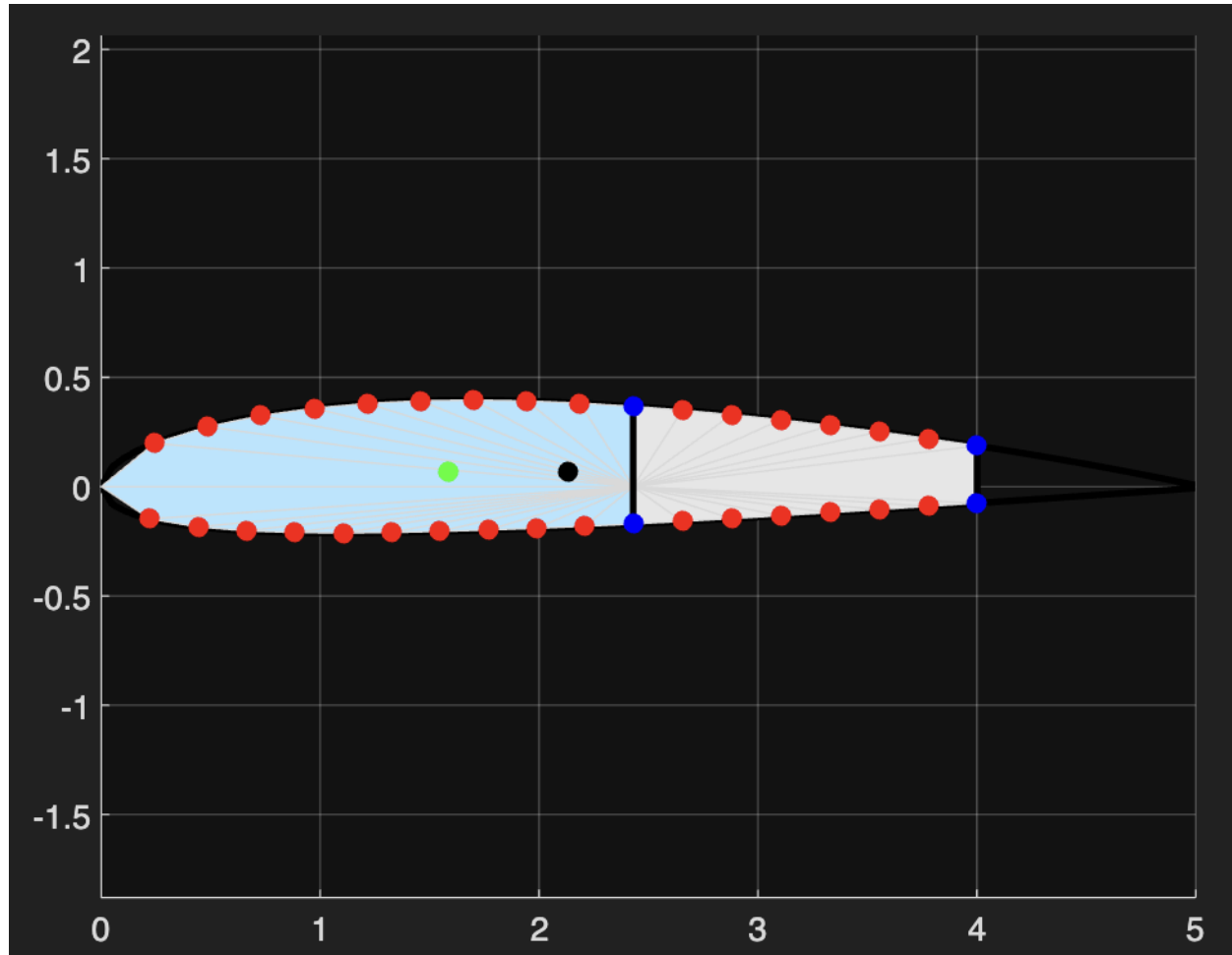


Figure 35. Histogram - Converged Wing Parameters



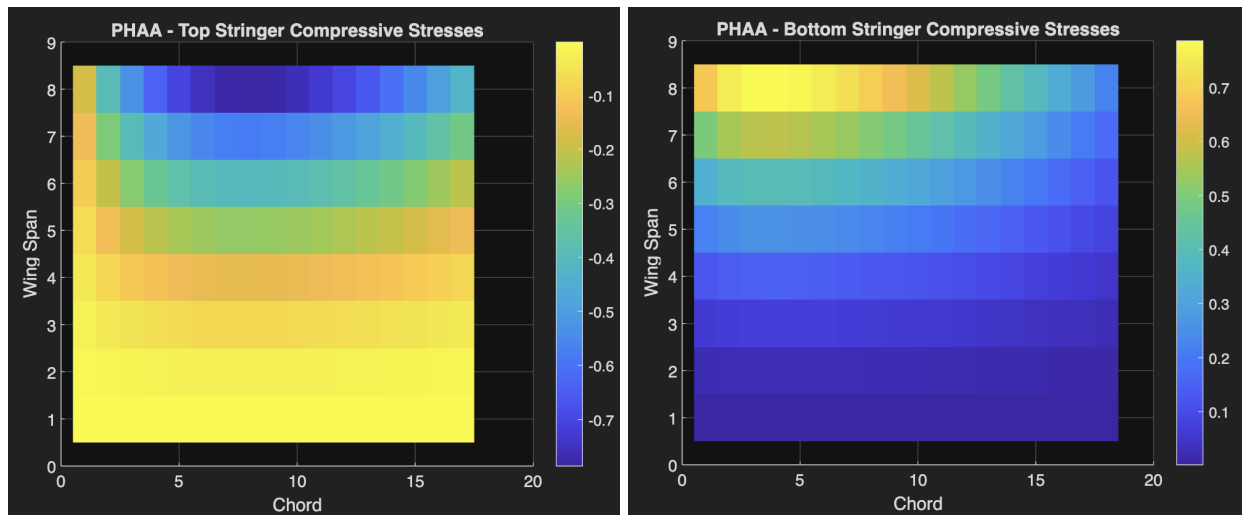
**Figure 36. Illustration of Final Wing Design**

| Wing Specifications                   |        |
|---------------------------------------|--------|
| Z-Stringer Area ( $\text{in}^2$ )     | 0.147  |
| Z-Stringer $I_{xx}$ ( $\text{in}^4$ ) | 0.0184 |
| Spar Cap Area ( $\text{in}^2$ )       | 0.147  |
| Spar Cap $I_{xx}$ ( $\text{in}^4$ )   | 0.0184 |
| # Top Stringers                       | 6      |
| # Bottom Stringers                    | 6      |
| # Nose Top Stringers                  | 9      |
| # Nose Bottom Stringers               | 10     |

|                         |        |
|-------------------------|--------|
| Panel Thickness (in)    | 0.0858 |
| Spar Thickness (in)     | 0.0868 |
| Front Spar Pos          | 0.4860 |
| Rear Spar Pos           | 0.8003 |
| # Ribs                  | 7      |
| Weight for 1 Wing (LBS) | 366    |

**Table 7. Final Wing Specifications****A. Stringer and Spar Cap Compressive Stresses Mesh Plot**

Figures 37-46 indicate that the wing design stringers maintain their bending/compressive integrity for all critical loads. The stress margin to failure becomes apparently lower in for PHAA and PLAA critical loading conditions, but do not exceed a failure ratio of 0.9. There is confidence in this design since a safety margin of 50% was already considered.

**Figure 37 & 38. PHAA Top & Bottom Stringer Compressive Stress Map**

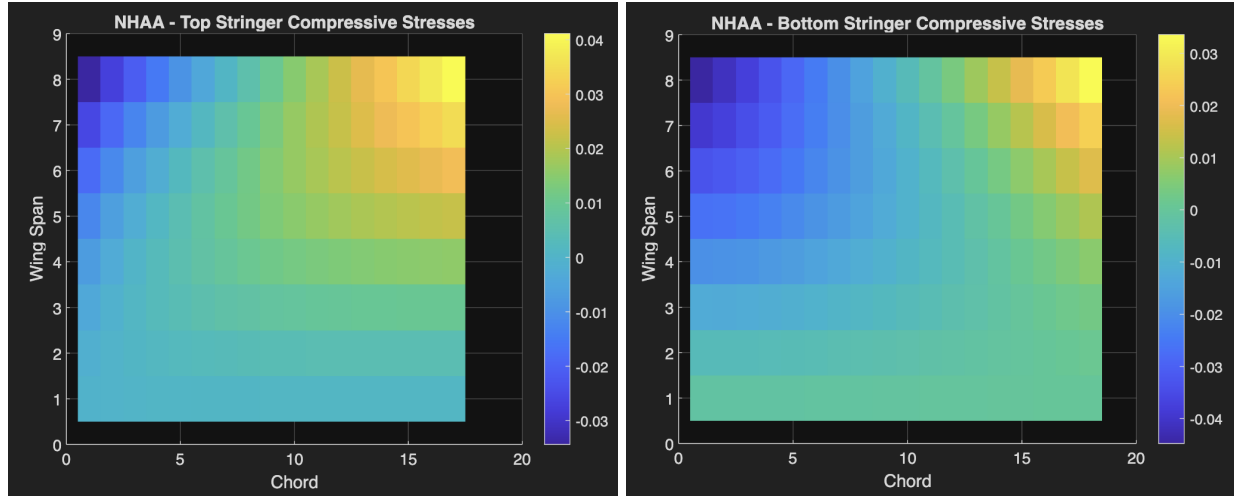


**Figure 39 & 40. NHAA Top & Bottom Stringer Compressive Stress Map**

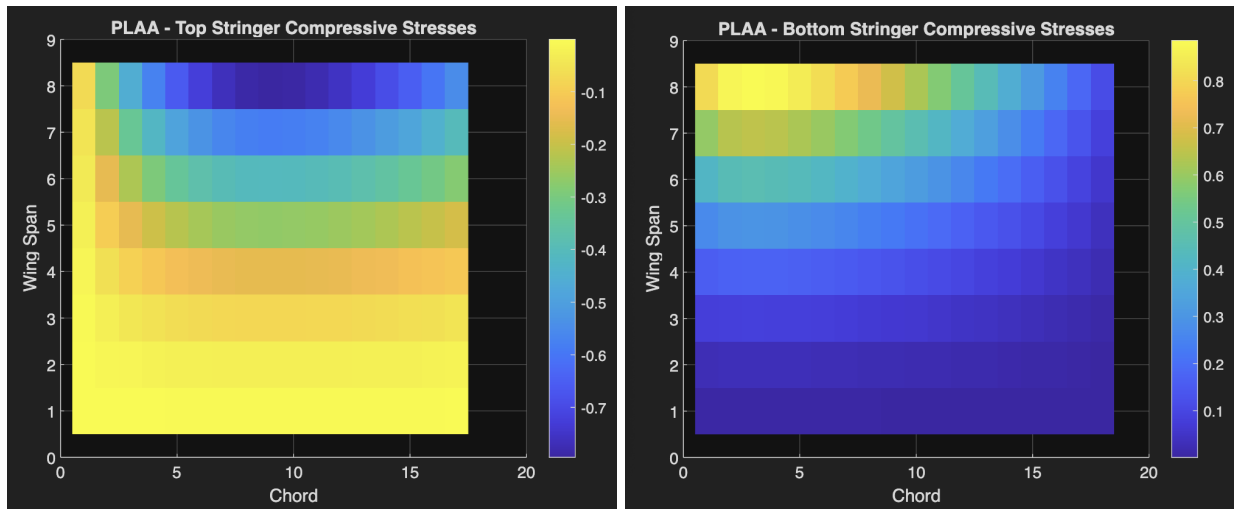


**Figure 41 & 42. PLAA Top & Bottom Stringer Compressive Stress Map**

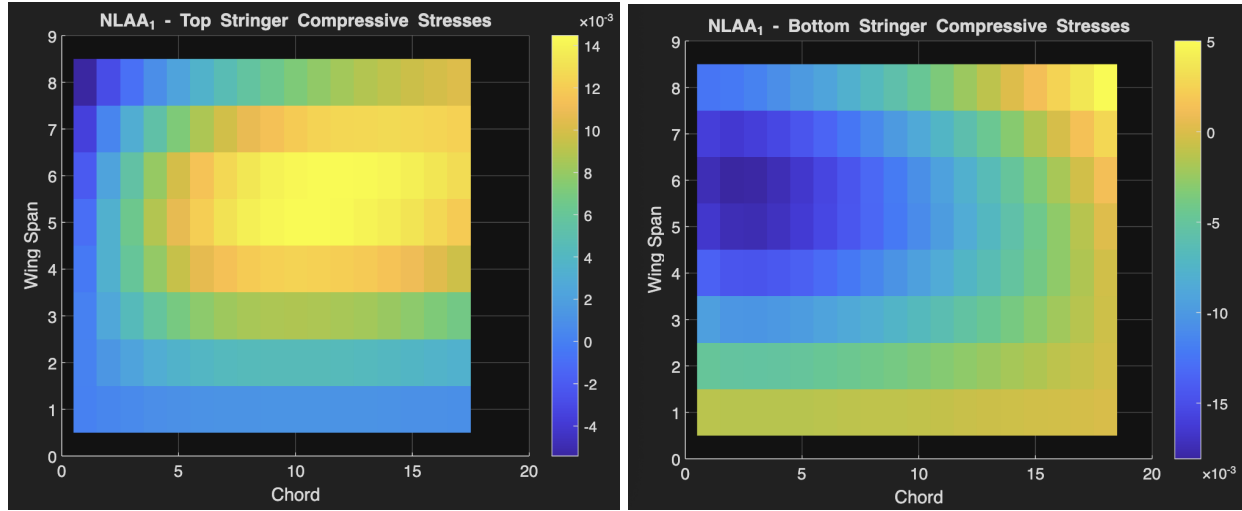


**Figure 43 & 44. NLAA<sub>1</sub> Top & Bottom Stringer Compressive Stress Map**

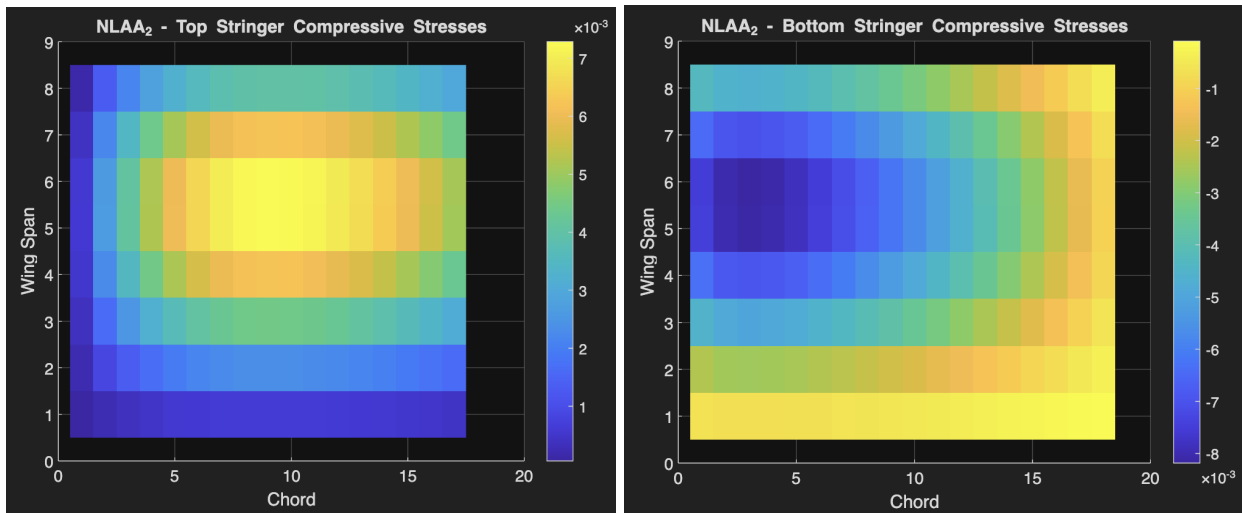


**Figure 45 & 46. NLAA<sub>2</sub> Top & Bottom Stringer Compressive Stress Map**

### B. Web Shear + Compressive Stresses Mesh Plot

Figures 47-56 indicate that the wing design stringers maintain their bending/compressive integrity for all critical loads. The stress margin of failure is the lowest for the webs under PHAA and PLAA loading conditions, but do not exceed a failure ratio of 1. There is confidence in this design since a safety margin of 50% was already considered.

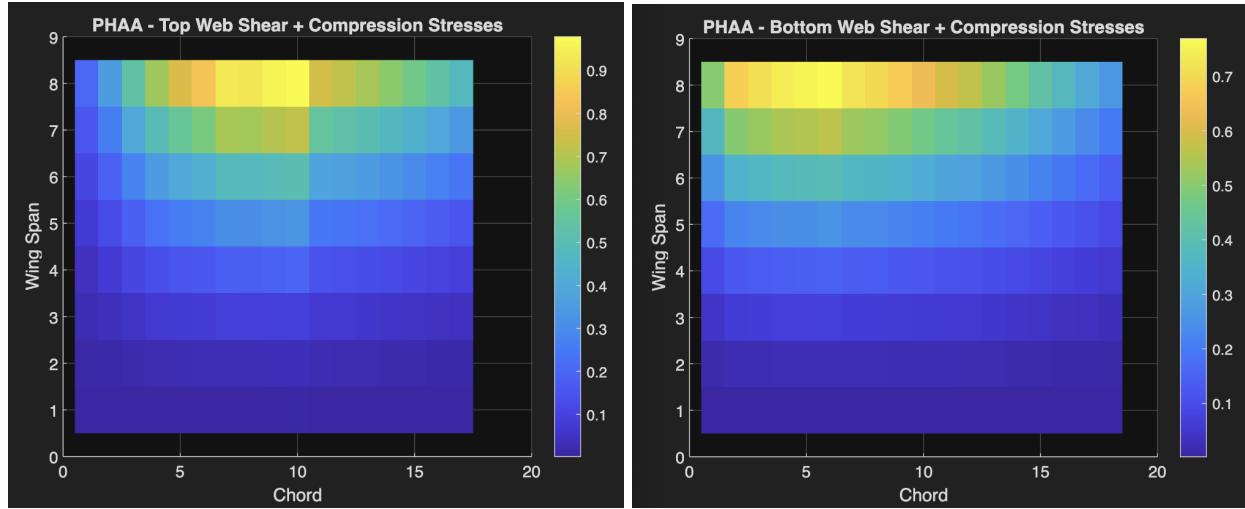


**Figure 47 & 48. PHAA Top & Bottom Web Shear + Compressive Stress Map**

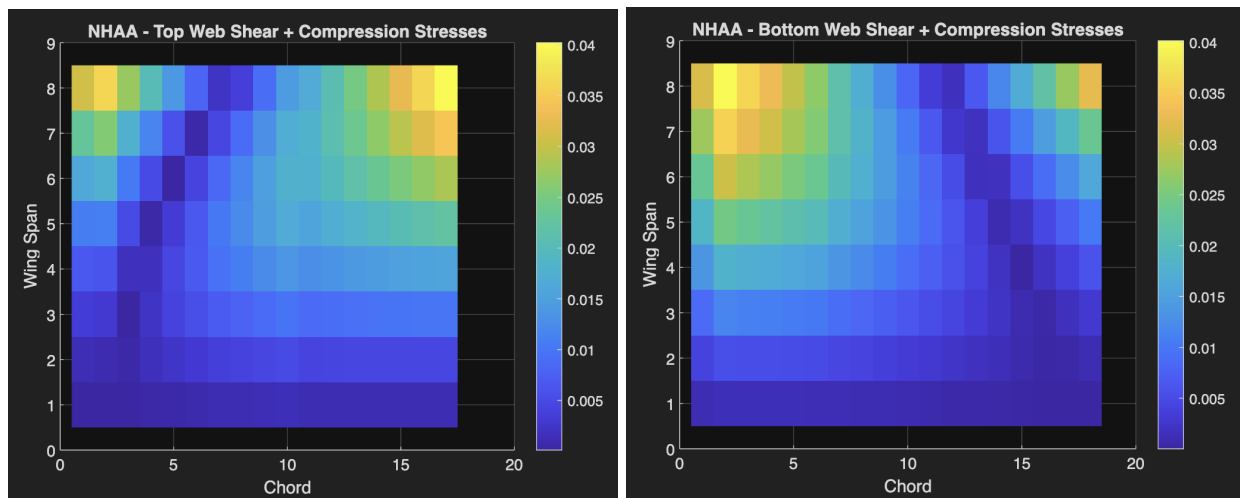


**Figure 49 & 50. NHAA Top & Bottom Web Shear + Compressive Stress Map**

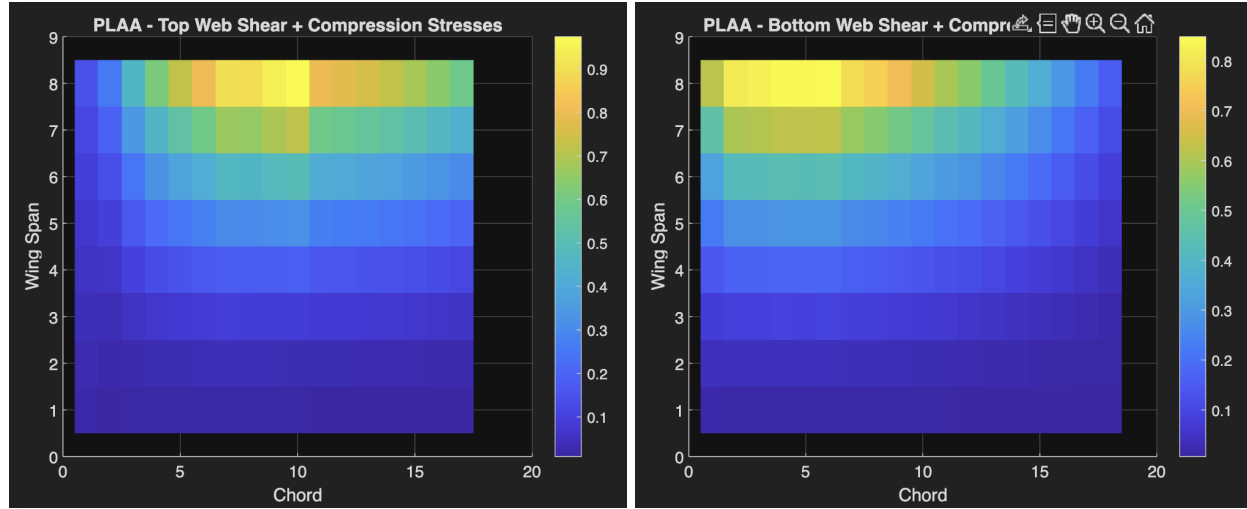


**Figure 51 & 52. PLAA Top & Bottom Web Shear + Compressive Stress Map**

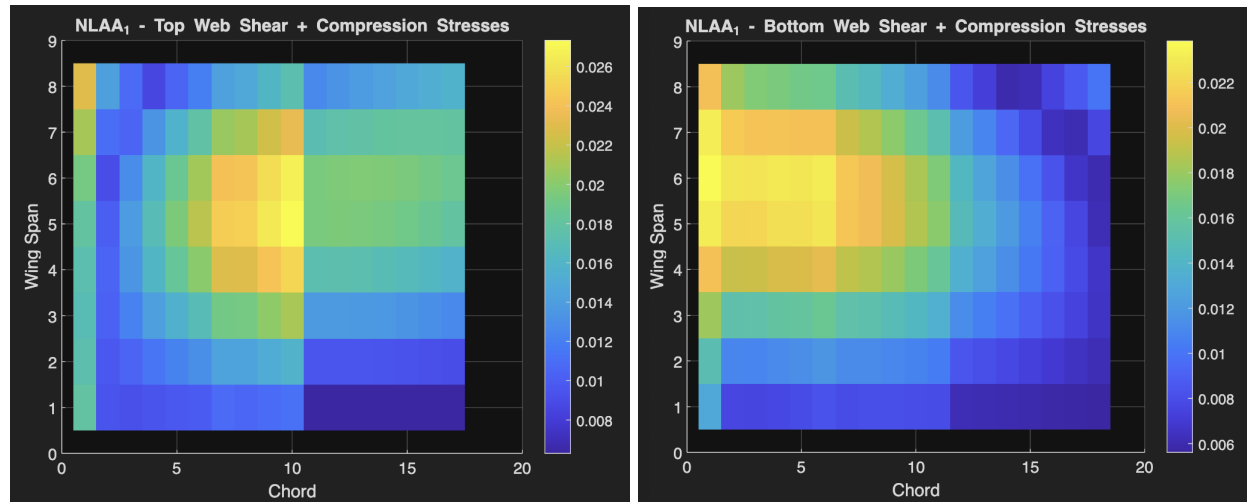


**Figure 53 & 54. NLAA<sub>1</sub> Top & Bottom Web Shear + Compressive Stress Map**

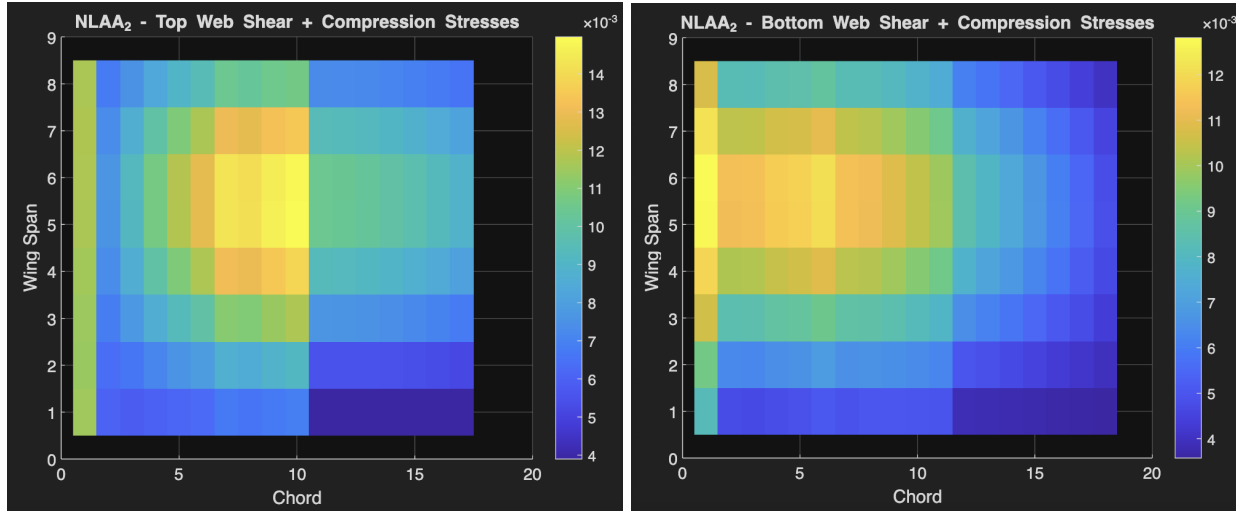


**Figure 55 & 56. NLAA<sub>2</sub> Top & Bottom Web Shear + Compressive Stress Map**

### C. Nose and Spar Shear + Bending Stresses Mesh Plots

These stress mesh plots, Figure 57-61, depict the stress margin gradient for the nose, front spar, and rear spar along the wing span. Although the spars do not indicate low margins to failure, they affect the structural and component integrity of the stringers/panels in their position along the chord. Front spar x position = 0.4860 and rear spar x position = 0.8003 were optimally curated per iterations.

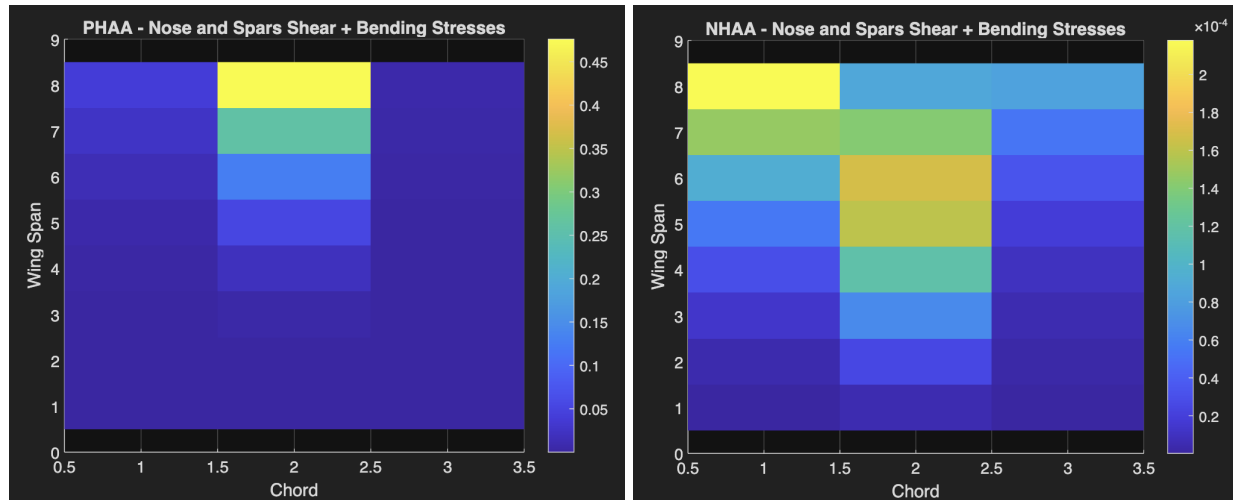


**Figure 57 & 58. PHAA/NHAA Nose & Spar Shear + Bending Stress Map**

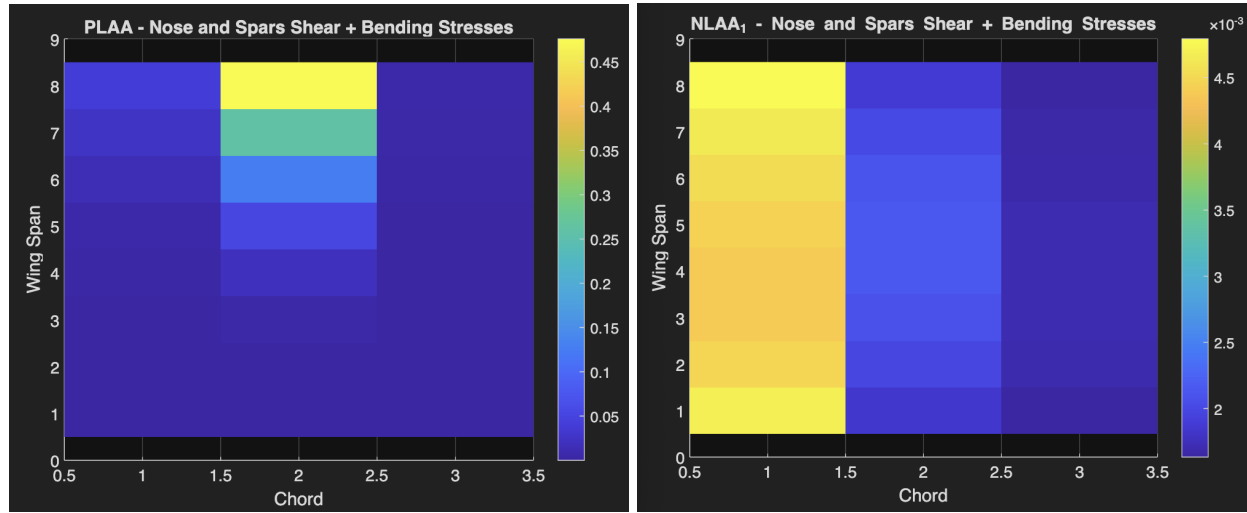


**Figure 59 & 60. PLAA/NLAA<sub>1</sub> Nose & Spar Shear + Bending Stress Map**

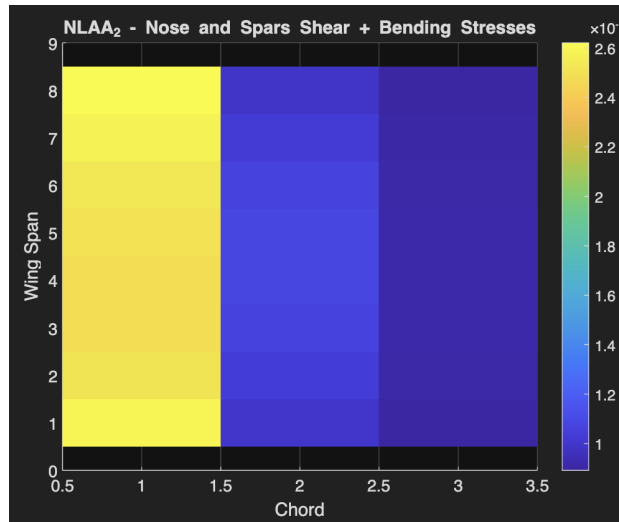


**Figure 61. NLAA<sub>2</sub> Nose & Spar Shear + Bending Stress Map**

#### D. Panel Yield Stresses Mesh Plots

As indicated by the colorbars in Figures 62-71, the stress margins to failure are objectively high. There is no concern for yielding failure.

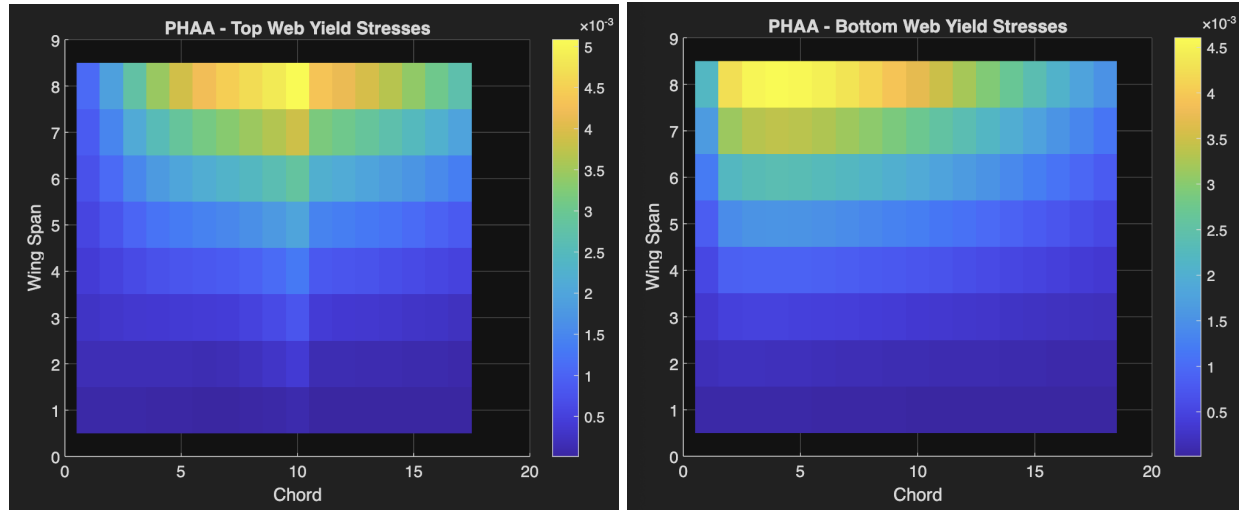


**Figure 62 & 63. PHAA Top & Bottom Yield Stress Map**

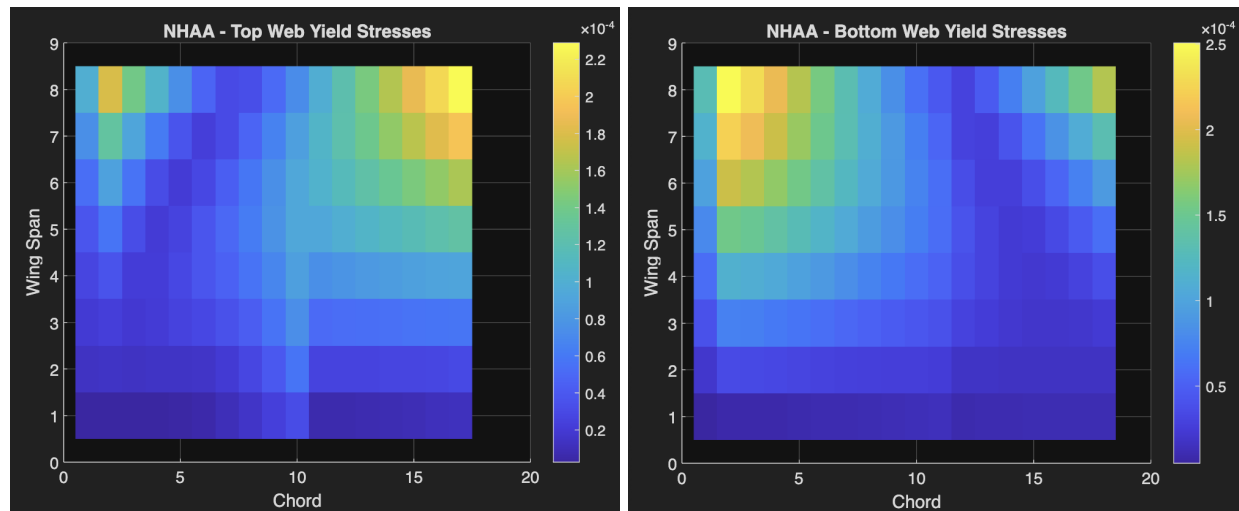


**Figure 64 & 65. NHAA Top & Bottom Yield Stress Map**

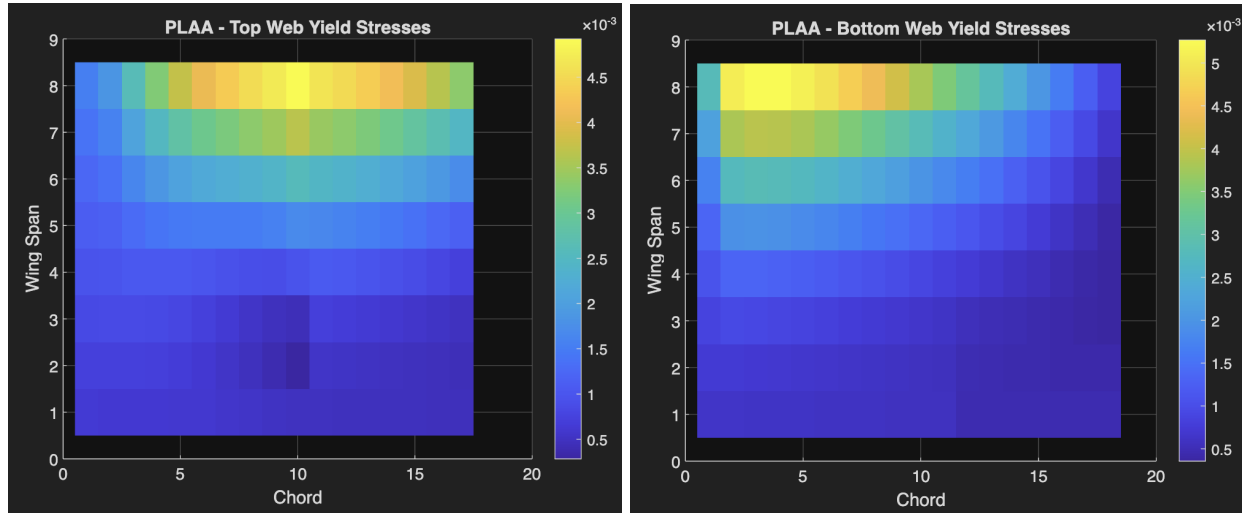


**Figure 66 & 67. PLAA Top & Bottom Yield Stress Map**

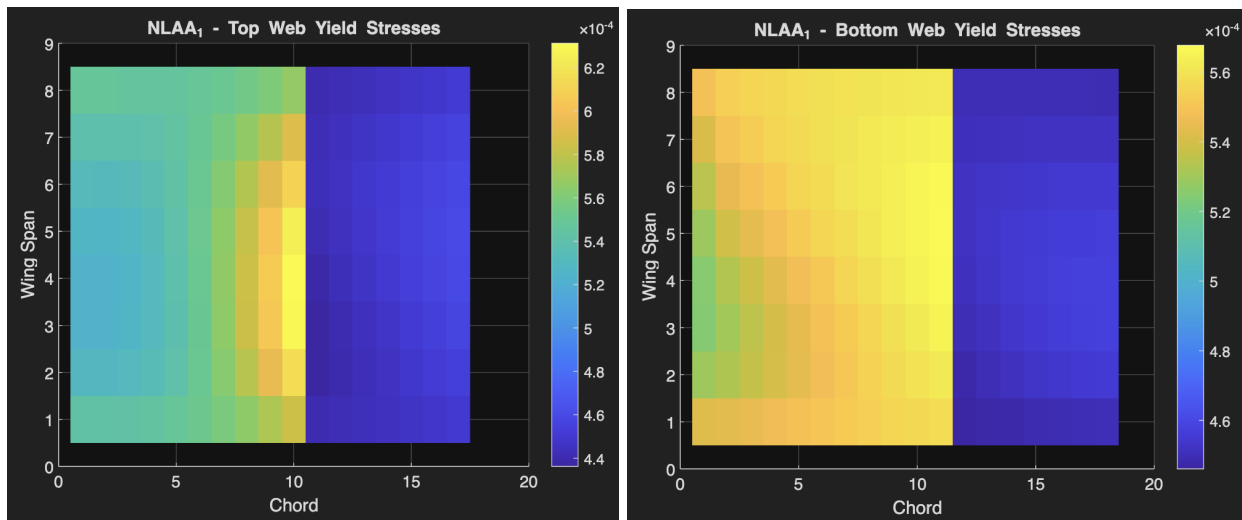


**Figure 68 & 69. NLAA<sub>1</sub> Top & Bottom Yield Stress Map**

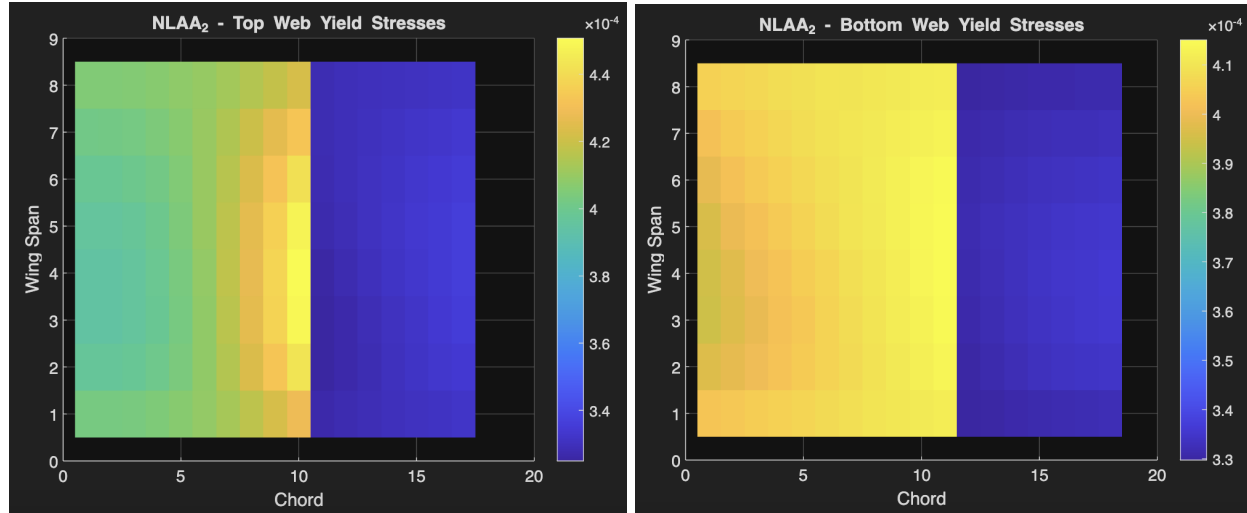


**Figure 70 & 71. NLAA<sub>2</sub> Top & Bottom Yield Stress Map**

The final wing design results in a total wing weight of 366 LBS for one wing, and hence 732 LBS for the entire wing structure. The lowest margin to failure is identified at the wing root panels (shear + compression combination stress) under loading conditions PHAA and PLAA critical loading conditions. The second lowest margin to failure is also located at the wing root stringers (compression stress) with respect to the same critical loading conditions, PHAA and PLAA. All stringers and webs all maintain a margin of safety  $<1$  with an additional safety margin of 50% applied to the stresses. The stress mesh plots, depicting the stress distribution across the wingspan, are reasonably patterned to match expected compression/tension, shear, and bending stress concentrations for respective critical loading conditions.

## X. CONCLUSION

Some improvements that can be made to determine a more weight-efficient wing design. First, the model accuracy can be further improved by involving the contribution of neglected variables that can be used to better simulate real-world applications (e.g. interference drag of the fuselage). Additionally, some wing design parameters remain consistent regardless of parameter quantity; instead, the design parameters could be expanded and defined. For example, all top panels share the same thickness dimension across the wing span. Material can be reallocated toward panels in higher stress concentration locations (this is the case for bottom, nose top, nose bottom, stringers, and spar caps as well). For the simplicity of this project, this improvement was not incorporated.

In summary, the final wing has been designed to operate under the applied lift and drag loads and analyzed to pass buckling, yielding, and wing divergence failure modes. One notable feature for the design is that the number of top and bottom nose stringers are relatively larger than the number of top and bottom body stringers. This instance was iteratively selected as an ideal feature to withstand higher aerodynamic and torsional loads under all flight conditions. This is also beneficially curated since this stiffens the nose of the wing to maintain the wing's aerodynamic shape by preventing deformation. As aforementioned, the structured Monte Carlo approach taken was efficient and effective. Although it takes a "brute-force" approach by consistently iterating large ranges of wing design parameters, it successively guarantees the functionality of the wing per iteration while consistently converging on an optimal wing design range parameters.